IMPROVEMENT OF INVERTED ORGANIC SOLAR CELLS BY COMBINATION OF GOLD QUANTUM DOTS AND PLASMONIC GRATING STRUCTURE

KULRISA KUNTAMUNG

DOCTORAL PROGRAM IN ELECTRICAL AND INFORMATION ENGINEERING
GRADUATE SCHOOL OF SCIENCE AND TECHNOLOGY
NIIGATA UNIVERSITY

ABSTRACT

In this study, we improve the light-harvesting efficiency of inverted organic solar cell (OSCs) through the combination of gold quantum dots (AuQDs) and grating-coupled surface plasmon resonance (GC-SPR). The constructed solar device comprises an ITO-coated glass substrate/titanium dioxide/poly(3-hexylthiophene-2,5-diyl):phenyl-C61-butyric acid methyl ester)/poly(3,4ethylenedioxythiophene):poly(styrene sulfonate):AuQDs/silver grating structure. The AuQDs are introduced into the hole transport layer (PEDOT:PSS) to increase the absorption in the ultraviolet (UV) light and near-UV light regions, which give rise to the light harvesting improvement of the devices in accordance to fluorescence. The plasmonic grating structures are created onto the active layer surface by nanoimprinting method using a PDMS stamp to induce the GC-SPR excitation within the devices. The UV-visible spectra, impedance spectra, current density versus voltage (*J*-*V*) characteristics, and atomic force microscopy images of the fabricated devices are investigated. The fluorescence from AuQDs incorporated into the GC-SPR evanescent field on the metal grating surface improves the short-circuit current density (*Jsc*) and the power conversion efficiency (PCE) in comparison to those of the reference cell and the cells with individual effects from AuQDs and metallic grating structures. The designed device shows an enhancement of photovoltaic efficiency achieved by increasing a PCE value from 3.25% (reference cell) to 3.77%, exhibiting an efficiency increase of 16%. Our results suggest that the improved efficiency of the inverted OSCs is achieved due to the combination of both G-AuQDs and GC-SPR.

Keywords: inverted organic solar cells, gold quantum dots, fluorescence, metallic grating structure, grating-coupled surface plasmon resonance, plasmon-enhanced fluorescence

ACKNOWLEDGEMENTS

Foremost, I would like to express my deepest sincere gratitude to Assoc. Prof. Dr. Akira Baba, and Asst. Prof. Dr. Kontad Ounnunkad for their giving great opportunity, kind supervision, valuable suggestions, practical training, continual encouragement, assistance, and financial support throughout this research work and helping me to succeed in this dissertation.

I am sincerely grateful to Prof. Dr. Keizo Kato, Prof. Dr. Kazunari Shinbo, Asst. Prof. Dr. Chutiparn Lertvachirapaiboon, and Prof. Dr. Futao Kaneko from Niigata University for impressive encouragement, insightful suggestion, practical training, and assistance.

I gratefully acknowledge Center for Transdisciplinary Research, Niigata University, Global Circus Program from Japan Society for the Promotion of Science (JSPS), Graduate School of Science and Technology Niigata University, and Human Resource Development in Science Project (Science Achievement Scholarship of Thailand, SAST) for financial supports.

Many thanks to my friends and colleagues for their help and warm friendship. Finally, I also gratefully acknowledge my beloved family for their unconditional love, understanding, encouragements and supporting throughout the period of my study. I would like to thank those whose names are not listed here, who have contributed to the success of this study.

Kulrisa Kuntamung

CONTENTS

CONTENTS (CONTINUED)

LIST OF TABLES

LIST OF FIGURES

LIST OF FIGURES (CONTINUED)

LIST OF FIGURES (CONTINUED)

LIST OF ABBREVIATIONS

AFM	Atomic force microscope
Ag	Silver
AgNPs	Silver nanoparticles
Al	Aluminum
AuNPs	Gold nanoparticles
AuNSs	Gold nanospheres
AuNRs	Gold nanorods
AuQDs	Gold quantum dot
BD-R	Blu-ray disc recordable
Ca	Calcium
DI water	Deionized water
DVD-R	DVD-ray discs
E.F.	Enhancement Factor
EIS	Electrochemical impedance spectroscopy
FF	Fill factor
FL	Fluorescence
GCSPR	Grating-coupled surface plasmon resonance
HOMO	Highest occupied molecular orbital
HTL	Hole transport layer
ITO	Indium-tin-oxide
IPCE	Photo to current conversion efficiency
J-V	Current-voltage
J_{sc}	Short-circuit current density
LSPR	Localized surface plasmon resonance
LUMO	Lowest unoccupied molecular orbital
NIR	Near-infrared
NPs	Nanoparticles
OSCs	Organic solar cells
P3HT	Poly(3-hexylthiophene)
PCBM	Phenyl-C61-butyric acid methyl ester

PCE	Power conversion efficiency
PDMS	Polydimethylsiloxane
PEDOT:PSS	Poly(3,4-ethylenedioxythiophene) polystyrene sulfonate
p-pol	*p*-polarize
R_s	Series resistance
R_{ct}	Charge transfer resistance
SPR	Surface plasmon resonance
SPPs	Surface plasmon polaritons
SP	Surface plasmon
s-pol	*s*-polarize
TiO_2	Titanium dioxide
UV	Ultraviolet
V_{oc}	Open-circuit voltage
V	Volt
Z	Impedance
^oC	Degree celsius
Ω	Ohm
π	pi bonds
η	Solar cell efficiency

CHAPTER 1

Introduction

1.1 Renewable energy demand

The demand for energy is increasing rapidly around the world. The effect of the economic development and population growth result in this increased demand. Fossil fuels, which include coal, gas, and oil are the major source of energy, which approximately 80 percent of the total energy consumption comes from these sources [1-3]. Most importantly, there are limited sources available, and they will run out in future [4]. Moreover, the combustion of fossil fuels releases large quantities of carbon dioxide, and other greenhouse gases such as nitrous oxide, methane into the atmosphere, which is the major cause of global climate change [3, 4]. To reduce the growth fossil fuels use, renewable energy sources play an essential role for the energy production and can effectively replace fossil fuels in the future. Renewable energy consumption has grown rapidly during the past decade, accounting for 12 percent of global total energy consumption in 2020 as illustrated in Figure 1.1 [5]. Renewable energy is also called green power or clean energy due to non-polluting source. There are five main types of renewable energy sources, depending on the resource being used [6, 7]. These are:

i. Solar energy (sunlight)
ii. Wind energy
iii. Hydropower (falling water)
iv. Geothermal power (the heat of the earth)
v. Biomass energy (plant materials)

Among these renewable energy sources, solar energy is considered one of the most popular alternative energy sources because it is the world's most abundant source of renewable energy that has great potential for placing the fossil fuel [8]. The photovoltaic cells, also called solar cells, can convert light (photons) from the sun to electricity (voltage) by the photovoltaic effect. Therefore, these devices are becoming increasingly important as a clean energy source.

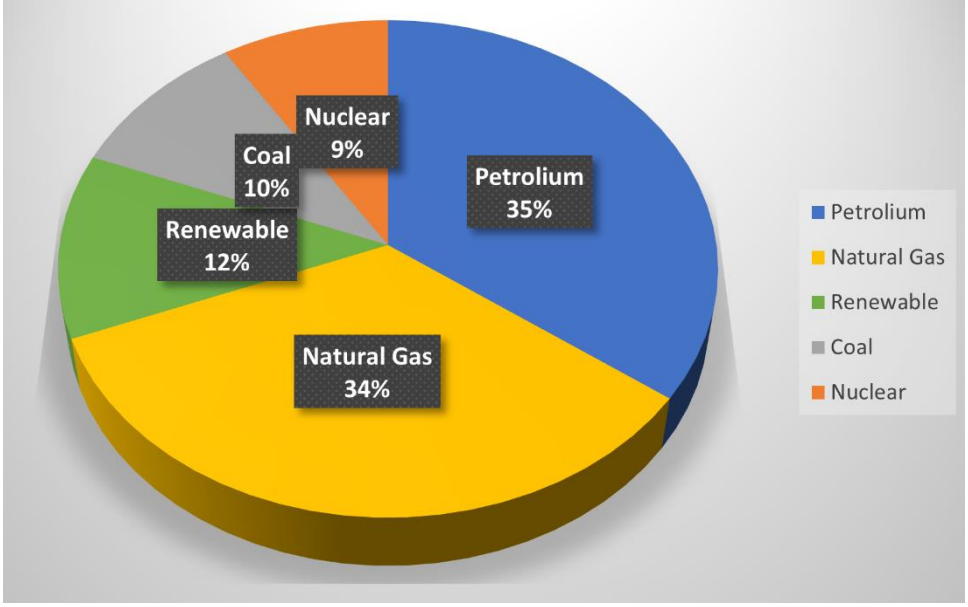

Figure 1.1. Energy consumption source.

The discovery of the photovoltaic effect began in 1839 with Edmond Becquerel, but the first practical photovoltaic cell was invented in 1954 at the Bell labs [9-11]. Photovoltaic technology can generate electricity directly from sun’s energy and is an important source of energy to produce energy in the future. This leads to increased interest in the development of efficient solar cells. Typically, photovoltaic system is of two main types depending on material, including inorganic solar cell using silicon and organic solar cell using organic materials [12]. Figure 1.2 shows an example of a ground mounted monocrystalline silicon array. Inorganic solar cells or silicon solar cells provide high power conversion efficiency (around 25%) and excellent lifetime (25-30 years) [12, 13]. However, there are some drawbacks such as

heavyweight, the high construction costs, and complex manufacturing processes [14]. Thus, the organic solar cells (OSCs) have attracted tremendous attention for potentially replacing inorganic solar cells owing to their potential inexpensive, light weight, easy fabrication method, and mechanical flexibility Moreover, many academic interests show that the OSCs are also a promising clean energy source. [13, 15-18].

Figure 1.2. Monocrystalline silicon photovoltaic array.

1.2 Organic solar cells

1.2.1 Principle of organic solar cells

OSCs utilize organic materials for converting sunlight into electricity via the photovoltaics process. Compared with inorganic solar cells, OSCs have several advantages, such as cheap, lightweight, non-toxic, flexible, and simple processing [13, 17, 19]. The first OSCs was produced by Dr. Ching Tang in 1986 [11]. The idea of employing organic materials is to replace the expensive traditional silicon solar cells. The OSCs differ from the traditional inorganic solar cells in term of the operating principles and the production methods. Small organic molecules or polymers are commonly employed for OSCs [19]. These molecules contain alternate single and double bonds resulting in the delocalization of electrons that can

help in effective electron transfer in the device. If these molecules are irradiated with light, the electrons will be excited from π bonding to π* antibonding state (π → π*). The π bonding represents the HOMO (highest occupied molecular orbital) while the π* antibonding is known as the LUMO (lowest unoccupied molecular orbital) [20, 21]. The energy difference between two orbitals corresponds to the band gap of organic semiconductor. The process of converting light energy into electrical energy in an OSC involves four important steps as shown below: [20, 22]

i. the light absorption to generate excitons (electron-hole pairs)
ii. the diffusion of excitons to active surface
iii. the exciton dissociation
iv. the transport of charge carriers to the electrodes and collection of the holes at the anode while electrons at the cathode.

The organic molecules or polymers are used in the active layers that act as electron donors or electron acceptors. The donor and acceptor materials are sandwiched between two electrodes, metallic electrode (Ag, Ca) and transparent electrode (indium Tin Oxide, ITO) [19]. Some of acceptor and donor materials for OSCs are displayed in Figure 1.3 [23]. In operating principle of the OSCs, the first step is photon absorption in the photoactive region (donor molecules), which leads to the formation of exciton. When the photon is absorbed by donor molecules, the excited electron will move into the LUMO energy level. Subsequently, the exciton diffuses to donor-acceptor interface, where it is separated into holes and electrons by the electric field. Lastly, the holes and electrons are then moved toward respective electrodes to produce the electric current as seen in Figure 1.4 [20, 23, 24]. PEDOT:PSS (poly(ethylenedioxythiophene) poly(styrene sulfonate)) is the conductive layer which can reduce the gap between the active layer and the anode [25].

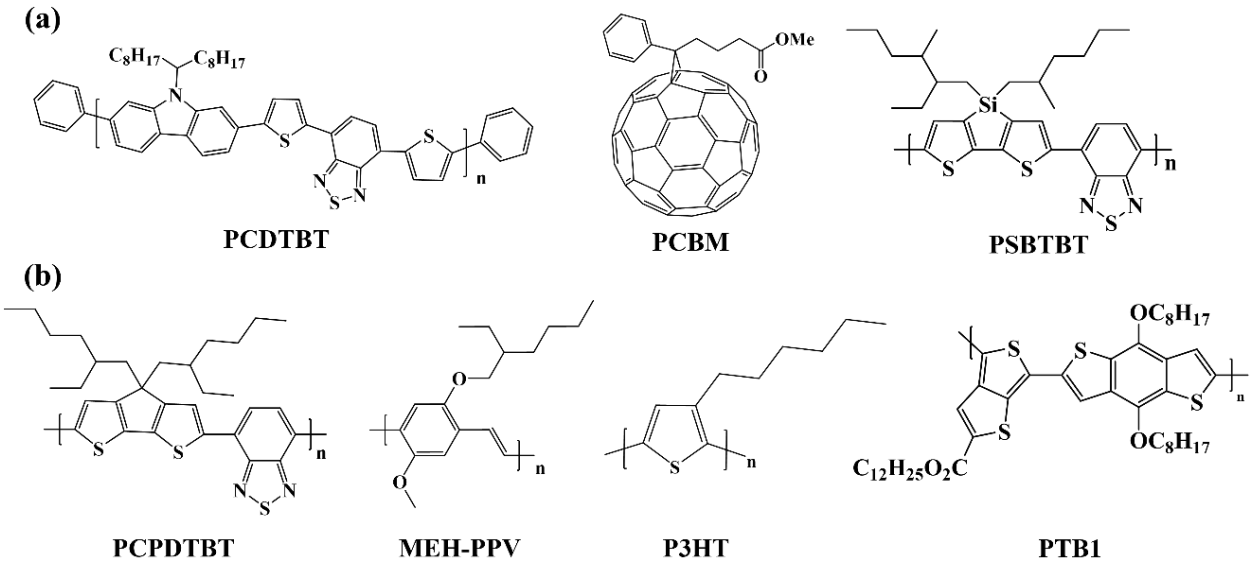

Figure 1.3 Chemical structures of (a) acceptor (b) and donor materials for OSCs.

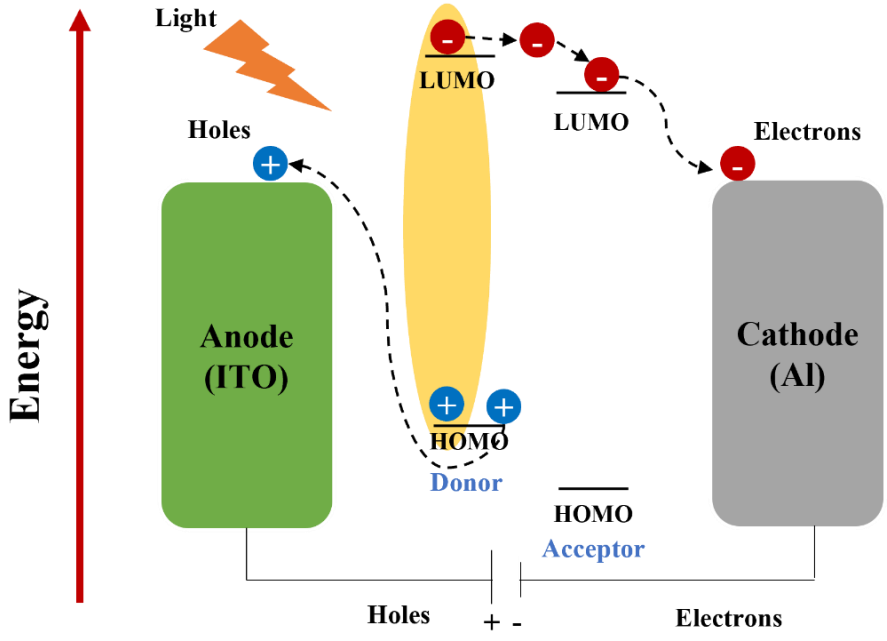

Figure 1.4. Working principle of organic solar cells.

1.2.2 Device structure of the organic solar cells

Typically, OSC is of three layers, including, metal cathode, transparent anode, and photoactive layer. The photoactive layer is inserted between two electrodes, namely, an anode and a cathode. The indium tin oxide or ITO is commonly employed as the anode layer for transparent electrodes. The cathode layer normally use metal electrode, namely, aluminum (Al) and calcium (Ca) [24]. Many researches have been studied to improve the efficiency of OSCs [26-31]. Figure 1.5 demonstrates the device structure of OSCs.

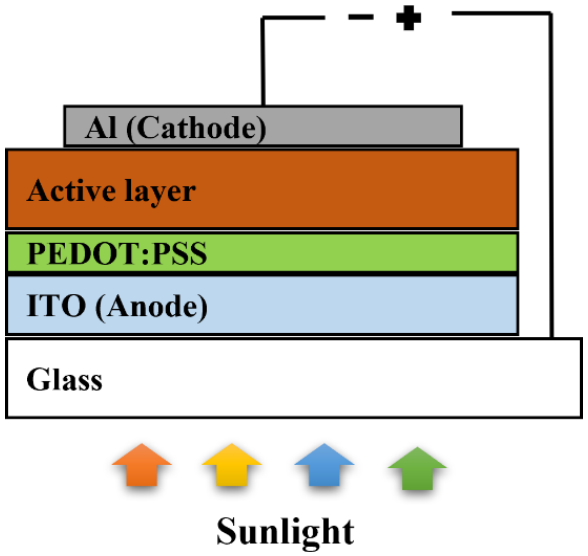

Figure 1.5. Typical device architecture of organic solar cell.

1.2.3 Photovoltaic parameters of organic solar cells

To characterize the OSCs performance, a *J-V* curve (current-voltage curve) is performed (see Figure 1.6). The important photovoltaic parameters can be extracted from the *J-V* plot, including *Jsc* (short circuit current density), V_{oc} (open circuit voltage), FF (fill factor), and PCE (power conversion efficiency). The *Jsc* is the current density at zero voltage per device area. The V_{oc} is the voltage generated by the cell at no current flow. The FF is the ratio between the actual maximum power obtainable from the cell and the theoretical power. The FF value can be calculated as illustrated in equation (1). The PCE plays a critical role in measuring the

performance and quality of OSCs. PCE is defined as the ratio of the energy output to the energy input. The equation to calculate the PCE value is shown in equation (2) [32, 33].

$$FF = \frac{Jmp \cdot Vmp}{Jsc \cdot Voc} \qquad \text{Equation 1}$$

$$\text{PCE\%} = \frac{Voc \cdot Jsc \cdot FF}{\text{Pinput}} \times 100\% \qquad \text{Equation 2}$$

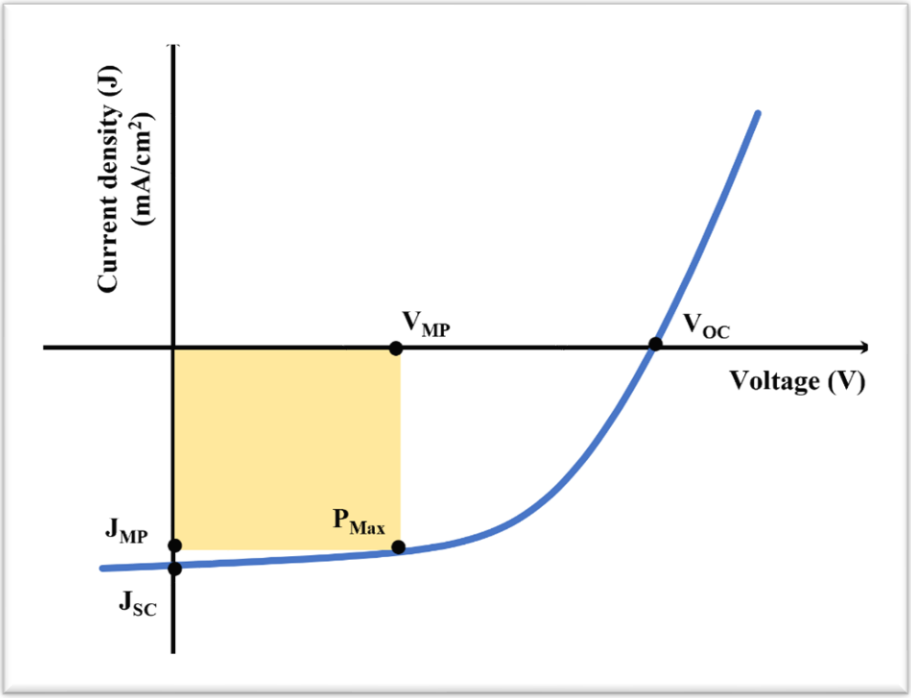

Figure 1.6. The *J-V* Curve of Photovoltaic characteristics of OSCs.

1.2.4 Inverted organic solar cells

The conventional and inverted OSCs are different systems in term of the light illumination pathway and device structure [24]. The inverted OSCs demonstrate with the light passing the semiconducting oxide before active layer. Although conventional OSCs are simple fabrication process, their fabrication use acidic PEDOT:PSS on ITO electrode, which is detrimental to the ITO surface, and the top low work function metal is air sensitive and easily oxidized, which result in poor durability of the devices [24, 34]. To improve the durability, stability and efficiency of the solar cell is by employing the inverted device structure. In

inverted solar cells (Inverted OSCs), the charge carriers move in an opposite direction when compared to the standard device, as illustrated in Figure 1.7. In standard solar cell, Al is widely used as cathode, which is easily oxidized in the air. For this reason, the gold or silver, which is the high work function metal, is used as the anode to extract holes while the transparent ITO electrode is used as the cathode to extract electrons from the active layer. Typically, a hole-blocking layer such as zinc oxide (ZnO) or titanium dioxide (TiO_2) is inserted between the ITO electrode and the active layer for hindering charge recombination [35].

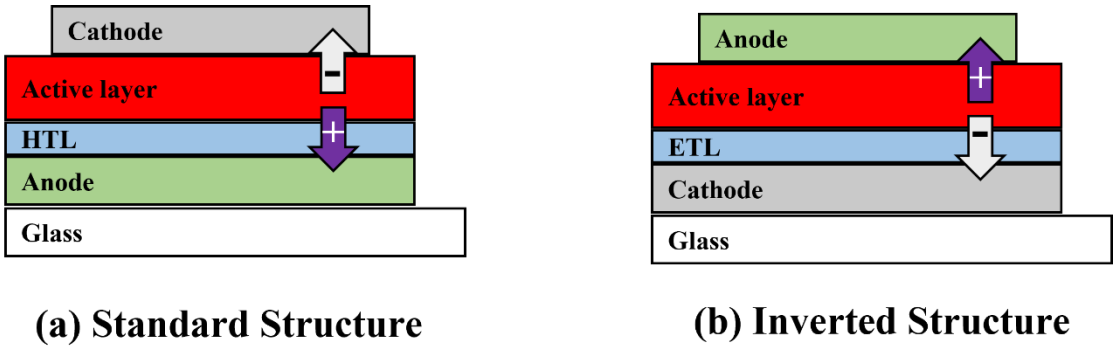

Figure 1.7. Comparison in direction of charge transport in (a) standard and (b) inverted OSC structures.

1.3 Approaches to enhance PCE in organic solar cells

The OSC has been continuously developed to improve the light harvesting performance; however, the lifetime and efficiency of OSC is still quite lower than the traditional solar cells and insufficient for commercial use. The performance of OSCs has been improved by many research groups by introducing plasmonic nanostructures, plasmonic nanoparticles, and quantum dot fluorescence, which can increase their device efficiency.

1.3.1 Incorporating with plasmonic nanostructures

Incorporating plasmonic nanostructures into solar cells is an alternative way for improving the devices performance. In OSC devices, most of the light can be absorbed by the active region. Therefore, increasing of the active layer thickness, light can be efficiently absorbed due to high absorption. Nevertheless, an increase in the active layer thickness will not increase the efficiency of the device. There is an optimum of the active layer thickness, which controls a balance between exciton diffusion length and light absorption. This limitation is due to the short exciton diffusion length in the photoactive layer which is typically less than 20 nm. Thus, larger thickness of the active layer can cause a higher recombination of the charge carriers in the photovoltaic cells, that possibly affect high resistance and low PCE. If active layer is very thin, it can lead to high optical losses due to insufficient light trapping. To boost efficiency, several researchers develop novel strategies that use metallic nanostructures to obtain effective light trapping ability for solar cell devices. The incorporation of metallic nanostructures into the solar cell device can increase the absorption of light without increase of the active layer thickness, reduce reflection, and enhance the optical path length of light for achieving highly efficient light harvesting [7, 17]. Surface plasmon polaritons (SPPs) occurs in plasmonic metallic nanostructures, which offers effective light trapping inside the photovoltaic devices. Figure 1.8 illustrates the plasmonic light-trapping by SPPs of textured surfaces.

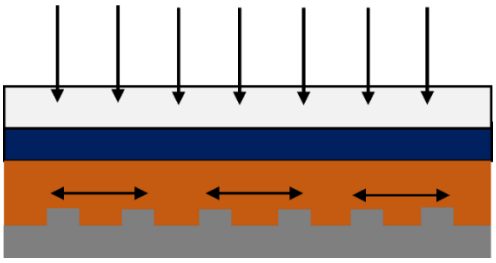

Figure 1.8. Plasmonic light-trapping by SPPs for OSCs.

1.3.2 Incorporating with plasmonic nanoparticles

Utilizing plasmonic nanoparticles are considered one of the promising approaches for increasing the light absorption in OSCs devices. The metal NPs (silver nanoparticles; AgNPs and gold nanoparticles; AuNPs) provide the absorption enhancement via light scattering and localized surface plasmon resonance (LSPR) effect. For the LSPR effect. it is produced by charge oscillation in metal NPs surface in presence of the electromagnetic field as shown in Figure 1.9. When the light illuminates on the metal NPs surface and matches the frequency with oscillation of the electron cloud. Then, the resonance frequency between electron cloud and photon is occurred resulting in the energy storage in the LSPR for metal NPs [36, 37].

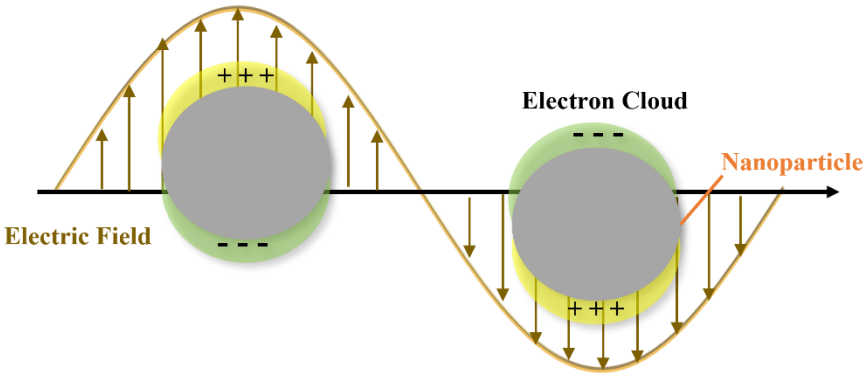

Figure 1.9. Illustration of electron cloud oscillation for LSPR of metal nanospheres.

In the case of OSCs as shown in Figure 1.10, incorporation of plasmonic metal NPs into the device can increase the light trapping of the photoactive layer in OSCs by two ways. Frist, the incident light is scattered within cell with large angle scattering, leading to increase the optical path length in the device, as seen in Figure 1.10a. In addition, metal NPs demonstrate for improving the light absorption due to the excitation of LSPR in metal NPs, which generates local electromagnetic field of the plasmonic solar cells, as seen in Figure 1.10b [7, 38].

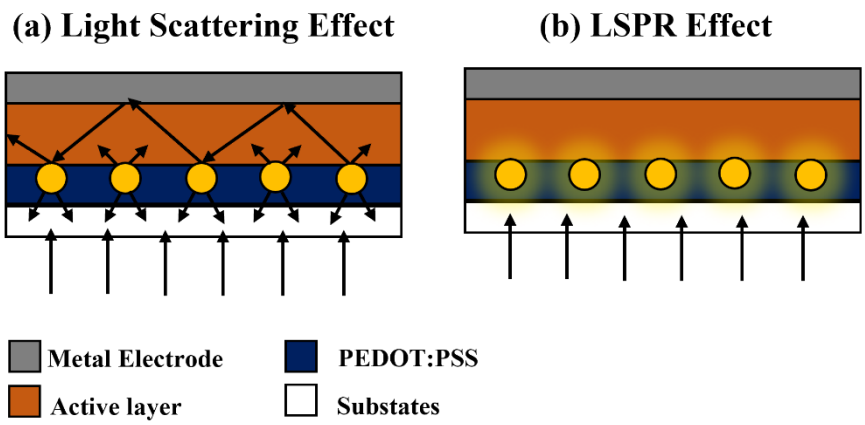

Figure 1.10. Plasmonic light-trapping architecture for OSCs, (a) light scattering, and (b) LSPR effect by metal NPs.

1.3.3 Incorporating with gold quantum dots

Gold quantum dots (AuQDs) have also been used to enhance PCE. Generally, AuNPs in the size ranges of 2-100 nm offer the plasmonic property. The particles sizes are smaller than 2 nm known as AuQDs, which are composed of 5 to 25 gold atoms. The decreasing particle size leads to an increase of bandgap energy and the conduction band and valence band split into quantized energy levels [39]. The electrons in the valence band of AuQDs absorb near-UV light and UV light, which are excited to the conduction band. Then, electrons can be return to the conduction band and after that the fluorescence emission in the visible region [40]. Figure 1.11 shows absorbance and fluorescence spectra of AuQDs. The AuQDs are mainly classified into several kinds according to size, composition, and structure. The properties of AuQDs lead to apply in many fields such as bioimaging, sensing applications, and solar cells [41]. Particularly, AuQDs can harvest the light from near-UV and UV regions and then convert to the fluorescence in visible regions, matching with the absorption range of of active layer. Thus, AuQDs are an alternative light emitting sources which can increase the light trapping within the devices.

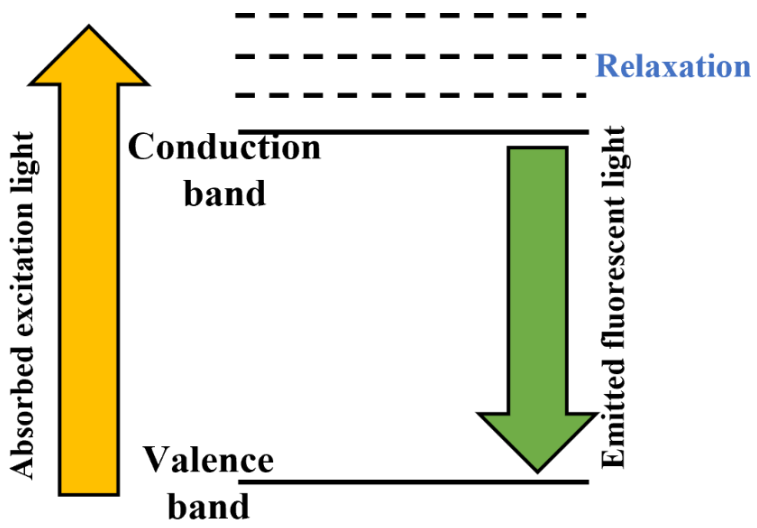

Figure 1.11. Absorbance and fluorescence diagram of AuQDs.

1.3.4 Incorporating with hybrid systems

Hybrid photovoltaic system is one of the promising approaches to enhance solar cell performance. Hybrid OSCs devices obtain different device structure, size and operating principle. Some of the different types are:

i. mixed metal NPs (AgNPs-AuNPs, AuNDs-AuNPs, AuNSs-AuNRs) [42-44] ;

ii. metal NPs (AuNPs, AgNPs, AgNDs, AgNSs)-grating structures [29];

iii. AuQDs-AuNPs [30];

iv. AuQDs-grating structures [31].

All developed solar cell provide the multiple effect and the synergistic effects within the devices, leading to an enhancement of the OSCs performance. For example, the combination of AuQDs and AuNPs obviously enhances electrical properties of solar cell device owing to the synergistic effect between the fluorescence phenomenon of AuQDs and the LSPR and/or the scattering effect of the AuNPs [30]. Moreover, incorporating AuQDs together with metallic nanostructures/gratings into OSC devices achieve high efficiency via synergistic effect of the fluorescence originated from AuQDs and GCSPR effect from plasmonic grating [31].

1.4 Research objectives

In previous studies, we have demonstrated that the combination of metal NPs and grating structures, AuQDs and AuNPs, AuQDs and grating structures into the conventional OSCs system can increase their device efficiency, then we attempt to develop inverted devices using materials mentioned above. Moreover, we have also reported improvement on performance of inverted OSCs using metallic nanostructures/gratings. This approach gives the light scattering and GCSPR effect, which lead to improve the efficiency of inverted OSCs. The combination of the AuQDs and plasmonic grating structures is expected to improve the performance of the inverted OSCs. Therefore, the objectives of this research are:

1. To fabricate and characterize the inverted OSC devices with high photovoltaic performances

2. To study the individual effects from AuQDs and GCSPR for light harvesting in inverted OSC

3. To study the effect of AuQDs incorporated with GCSPR for improving efficiency of inverted OSC device.

CHAPTER 2

EXPERIMENTAL SECTION

2.1 Chemicals and materials

Table 2.1 Chemicals and materials, molecular weight, purity and company.

Chemicals and materials	molecular weight	purity	company
Gold quantum dots (B-AuQDs, G-AuQDs, and R-AuQDs)	- B-AuQDs (mixed 5 and 8 Au atoms) - G-AuQDs (13 Au atoms) - R-AuQDs (25 Au atoms)	-	Dai Nippon (Japan)
Poly(3,4-ethylenedioxythiophene): poly(styrene sulfonate) (PEDOT:PSS, CleviosTM HTL Solar)	-	-	Heraeus (Germany)
Poly(3-hexylthiophene-2,5-diyl) (P3HT)	50,000-100,000	> 99%	Sigma-Aldrich (Japan)
[6,6]-Phenyl C61 butyric acid methyl ester (PCBM)	910.88	> 99%	Sigma-Aldrich (Japan)
Nitric acid (HNO_3)	63.01	60%	Sigma-Aldrich (Japan)
Hydrochloric acid (HCl)	36.46	37%	Sigma-Aldrich (Japan)
Titanium tetrabutoxide	340.32	97%	Sigma-Aldrich (Japan)
1,2-dichlorobenzene	147.00	99%	Sigma-Aldrich (Japan)

Table 2.1 (cont.) Chemical and materials, molecular weight, purity and company.

Chemicals and materials	molecular weight	purity	company
Ethanol (C_2H_5OH)	46.08	99.5%	Sigma-Aldrich (Japan)
Acetone	58.08	AR grade	Sigma-Aldrich (Japan)
Indium tin oxide (ITO) coated glass slide (conductivity of 10 Ω/cm^2)	-	-	Furuuchi chemical (Japan)

2.2 Instruments

Table 2.2 Instruments, model and company.

Instruments	Model	Company
Ultrasonic bath	D-78224 Transonic Digitals	Elma
Oven	Memmert 70	Memmert
Atomic force microscope (AFM)	SPM-9600	SHIMADZU
Potentiostat set	HZ-5000	Hokuto Denko Ltd.
Solar simulator (AM1.5)	HAL-C100	Asahi Spectra
Scanning electron microscope (SEM)	JSM6335F	JEOL
UV-vis spectrophotometer (UV-vis)	V-650	Jasco
Spin coater	1H-D3	Misaka
UV/Ozone Cleaning Equipment	ASM401N	ASUMI GIKEN Limited

2.3 Cleaning of indium tin oxide (ITO)-coated glass

The first step for any device fabrication process is cleaning substrates prior to the deposition of all other layers. The ITO-coated glass with resistance of 10 Ω/cm^2 were cut to a size of 2 × 2.5 cm. ITO patterns were etched by HCl etching process. Then, the ITO electrodes were sonicated for 20 min in detergent, tap water, and two time of deionized (DI) water, respectively. After that, ITO substrates were dried at 60 ºC for 3 h in an oven. In order to pattern the cell area, ITO substrates were covered with tape (Scotch 3M) to have the cell area of 1.0 cm^2. Finally, the cleaned substrates were treated for 45 min using ultraviolet (UV)/ozone cleaner to remove organic contamination, as shown in Figure 2.1. These substrates were ready for coating next layers.

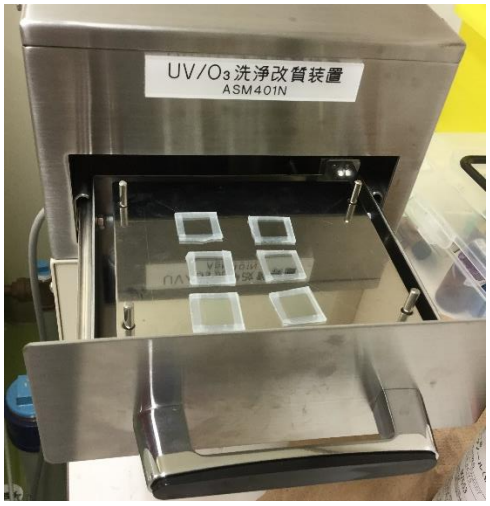

Figure 2.1 The UV Ozone treatment for the preparation of ITO glass substrates.

2.4 Preparation of the DVD-R and BD-R grating master template

BD-R discs (Blu-ray disc recordable, grating pitch = 320 nm) were cut to small pieces and soaked for 20 min in the concentrated nitric acid to eliminate the metal coated BD-R. After that, BD-R pieces were cleaned by sonicating in detergent, tap water, and DI water, sequentially and then dried in a nitrogen gas flow. In preparation for DVD-ray discs (DVD-R, Λ = 740 nm),

they were cut into several pieces and immersed in ethanol for approximate 15 min to eliminate the organic dye coating from DVD-R. Then, pieces of the DVD-R were washed by sonicating in detergent, tap water, and DI-water, respectively. Figure 2.2 shows AFM images of BD-R and DVD-R grating master template.

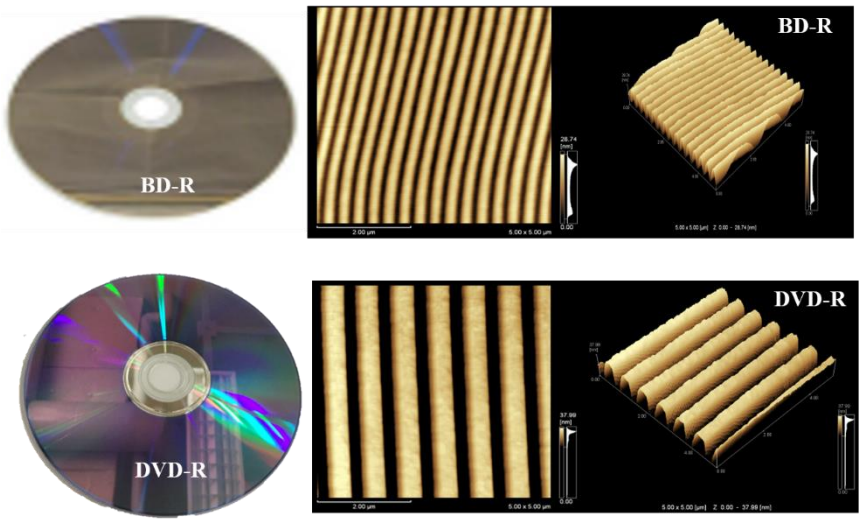

Figure 2.2 AFM images of the BD-R and DVD-R grating master template.

2.5 Preparation of the PDMS grating molds

To obtain liquid polydimethylsiloxane (PDMS), the sylgard 184 silicone elastomer base and silicone elastomer curing agent were mixed together (weight ratio: 10:1). Next, liquid PDMS was degassed and then poured on top of the cleaned BD-R and DVD-R, which were employed as diffraction grating substrates. Then, they were placed in a vacuum chamber for 2 hours to release any trapped air bubbles, followed by curing for 1 hours at 79 °C. After curing, the PDMS stamp with negative patterns of BD-R and DVD-R structures were obtained and employed to transfer the grating pattern on the photoactive layer surface of the solar cell devices, as shown in Figure 2.3.

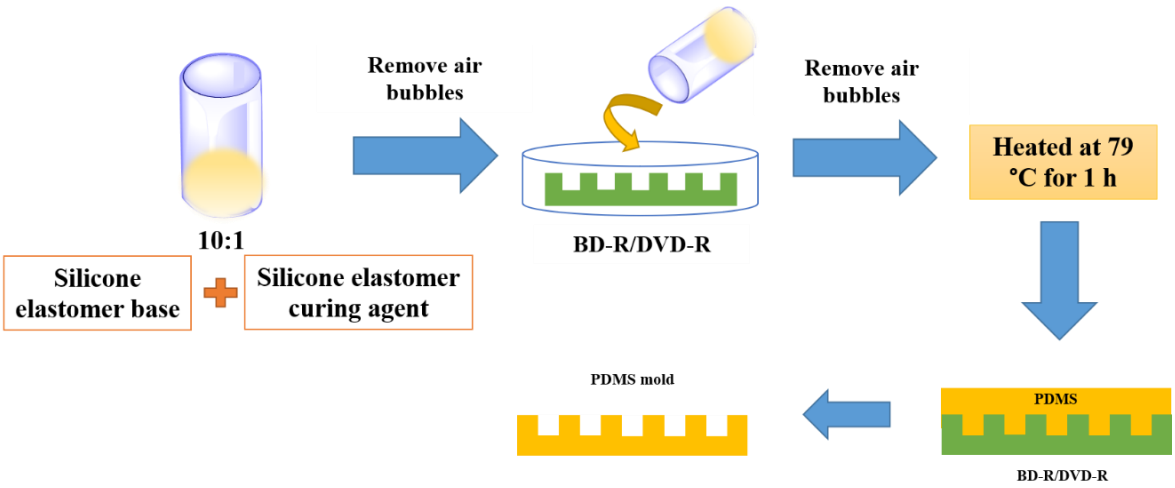

Figure 2.3 Illustration of the preparation of PDMS grating mold.

2.6 Synthesis of the TiO_2

The modified sol-gel method was used to synthesize titanium dioxide (TiO_2). Firstly, 250 µL of titanium (IV) butoxide [$Ti(C_4H_9O)_4$], which was used as a titanium precursor, was added to 5.0 mL of ethanol, and stirred for 1 h. Secondly, 150 µL of DI water containing 25 µL of HNO_3 was added to the above titanium butoxide in ethanol solution. Then, the mixture solution was stirred for 3 h at room temperature. The TiO_2 solution was obtained after aging for 24 h at room temperature. The synthesis of TiO_2 is provided in Figure 2.4.

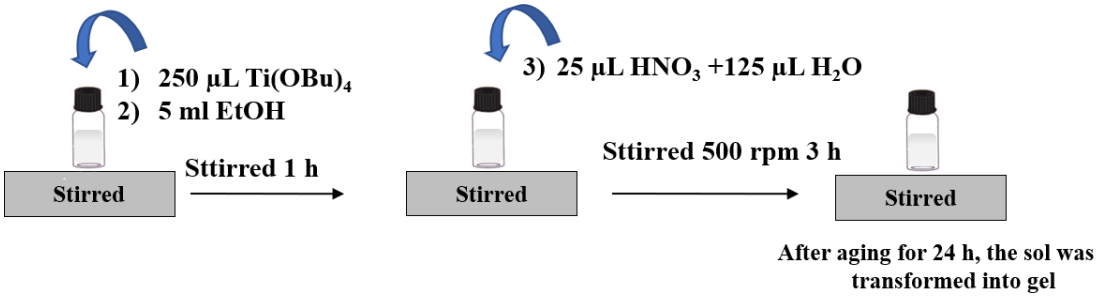

Figure 2.4 The synthesis of TiO_2.

2.7 Design and fabrication of inverted OSC structure

Figure 2.5. shows the device architecture of inverted OSCs with the AuQDs alone (Figure 2.5 left), metallic grating structures alone (Figure 2.5 right), and the grating structures in the presence of AuQDs (Figure 2.5 bottom). The constructed solar device consisting of ITO/TiO_2/P3HT:PCBM/PEDOT:PSS:AuQDs/Ag grating structures was used in this study.

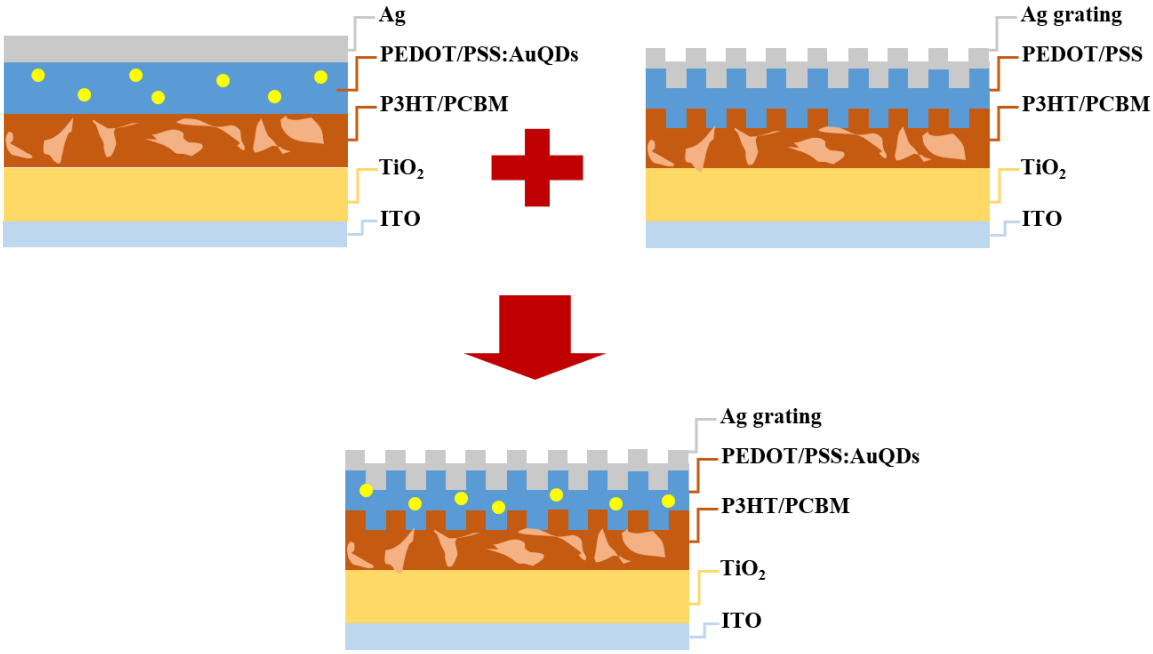

Figure 2.5 The inverted OSCs device architecture.

The basis of producing solar device, the cleaned ITO glass substrate was firstly placed in the UV/ozone cleaner for 45 min before deposition of the organic layers. The substrate was mounted on a rotation plate of the spin coater. TiO_2 solution was coated on ITO glass substrate by spin coating method for spinning rate of 2,000 rpm for 60 s. The prepared TiO_2/ITO substrate was preheated at 100 °C for 10 min to eliminate residual solvent. The TiO_2 film was subsequently placed on a hotplate and heated to 400 °C for 30 min to convert the TiO_2 to crystalline phase. This step was repeated two times to get the desired coating thickness. Then, the active layer was prepared by dissolving P3HT:PCBM (1:0.8 of weight ratio) in 1,2-

dichlorobenzene. The mixture solution was sonicated overnight at room temperature. The blended solution of P3HT:PCBM was spin-coated on the TiO_2 thin film coated substrate at two different rotating speeds of 1500 rpm for 20 s and at 2000 rpm 40 s, followed by thermal annealing at 100 °C for 1 h to form the active film on the inverted OSC device. Next, the grating patterns (DVD-R or BD-R) were created on the P3HT:PCBM layer by the nanoimprinting technique using a PDMS mold as a template. All air bubbles in the gap between the active layer film and PDMS mold were removed by vacuuming and it was heated at 100°C for 1 h. Subsequently, it was kept at room temperature to cool down and the PDMS layer can be peeled off from the device. The solution of PEDOT:PSS was mixed with AuQDs solution (G-AuQDs, B-AuQDs or R-AuQDs) (1:6 v/v) and sonicated for 1 h in an ultrasonic bath as shown in Figure 2.6. After that, the mixture solution of PEDOT:PSS:AuQDs was deposited on a grating patterned active layer by spin coating speed 1500 rpm and spinning time 90 s to form hole-transport layer, and the film was then heated at 120°C for 10 min Lastly, the 150 nm silver film was deposited onto the surface of PEDOT:PSS:AuQDs layer using a thermal evaporation to work as top electrode. To achieve a good contact between each layer of the device, ITO/TiO_2/P3HT:PCBM/PEDOT:PSS:AuQDs/Ag grating structure was dried by a vacuum chamber at 150 °C for 45 min. The fabrication process and structure of the inverted OSC device is shown in Figure 2.7.

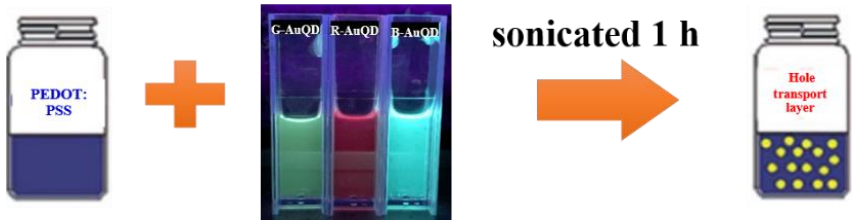

Figure 2.6 The preparation of the AuQDs-loaded PEDOT:PSS layers.

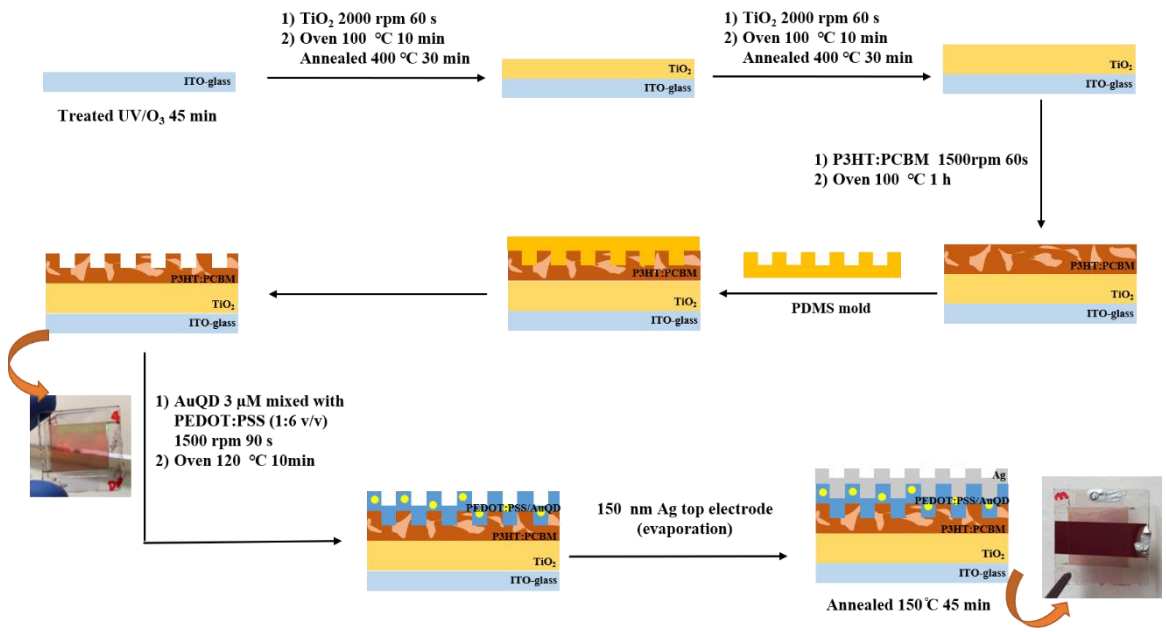

Figure 2.7 Schematic illustration for of the fabrication process of the inverted OSC device.

2.8 Device characterization

The HR 4000 spectrometer (Ocean Optics, Inc.) was used to measure the fluorescence emission spectra, including G-AuQDs, PEDOT:PSS, and G-AuQDs/PEDOT:PSS aqueous solutions. The SPR and fluorescence properties of the G-AuQDs/PEDOT:PSS film on an metallic grating were investigated by a photomultiplier tube (PMT) system with the devices mounted behind the sample holder. The SPR and fluorescent measurements were performed at different incident angle and a fixed wavelength at 510 nm, as shown in Figure 2.8. The surface morphologies of the inverted OSC were observed by an atomic force microscope (AFM, SPM 9600 from Shimadzu, Japan). The photocurrent properties of the developed device were measured by an electrometer (B2901 from Agilent). Electrochemical impedance spectroscopy (EIS) measurement was performed using PARSTAT 4000 from Princeton Applied Research at frequency ranging from 1 Hz - 1 MHz with an excitation amplitude of 10 mV. The devices were illuminated by a solar simulator (HAL-C100 from Asahi Spectra USA Inc.) with the intensity of 75 mW/cm^2. A picture of the instrumentation is shown in Figure 2.9. For the

reflectivity characterization, the fabricated device was fixed on a θ-2θ goniometer stage. The device was irradiated by polarized white light, which was generated from a halogen lamp. The SP excitation experiment was carried out at a fixed incident angle as a function of the wavelength.

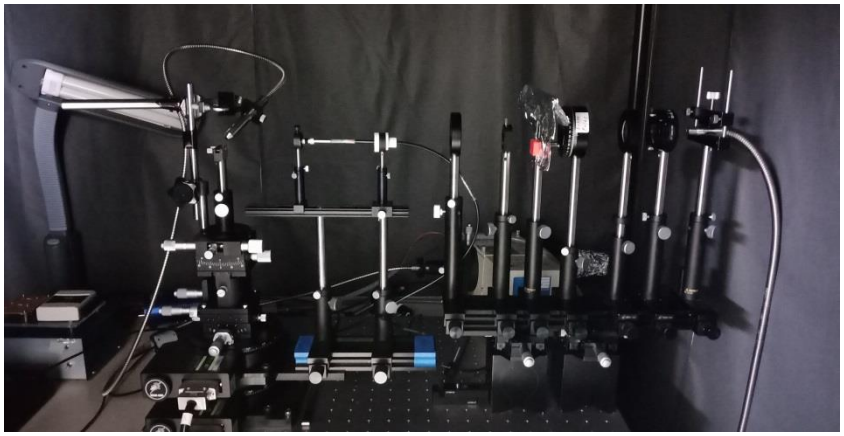

Figure 2.8 Picture of the SPR fluorescence spectroscopy instrumentation.

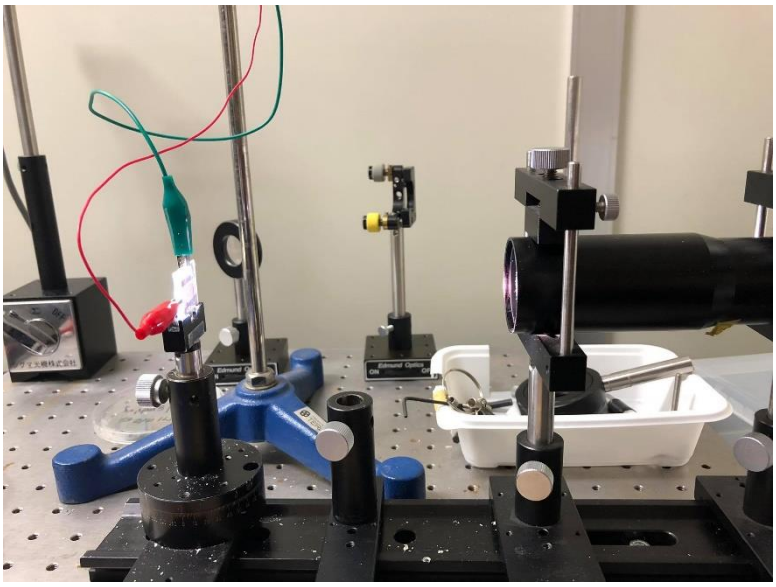

Figure 2.9 The photocurrent measurement apparatus for the developed inverted OSC devices.

CHAPTER 3

RESULTS AND DISCUSSION

3.1 Effects of three types of AuQDs

First, we focus on the size and concentration effect of AuQDs used in flat inverted OSC devices to achieve higher light harvesting efficiency as compared to that of reference cell without AuQDs. The AuQDs can be incorporated into the devices by their dispersion in HTL layer. AuQDs are classified into three types according to their size, including B-AuQDs (mixture of Au5 and Au8), G-AuQDs (Au13), and R-AuQDs (Au25). Three different sizes of AuQDs show different fluorescent colors that affect the performance of inverted OSC devices [45]. Incorporating AuQDs into inverted OSCs is expected to improve light trapping due to the emitted visible light from the AuQDs. To study the concentration of three types of AuQDs, they are blended in the PEDOT:PSS solution and varied in the range of 0.14-1.00 µM as seen in Figure 3.1. In all cases with AuQDs show the highest efficiency at 0.43 µM. The efficiencies slightly increase when increasing the concentration of AuQDs from 0.14-0.43 µM and then decrease at higher concentration. The decreased efficiency may result from the aggregation of AuQDs at higher concentration [27]. The large aggregates are found in the case of B-AuQDs, that can cause decreased device efficiency in comparison with G-AuQDs, which is similar to the result in a previous study [27]. Furthermore, G-AuQDs offer the fluorescence emission, which can be harvested by the P3HT:PCBM region, thus giving the maximal value of PCE [30]. Thus, G-AuQDs concentration of 0.43 µM is chosen for next study.

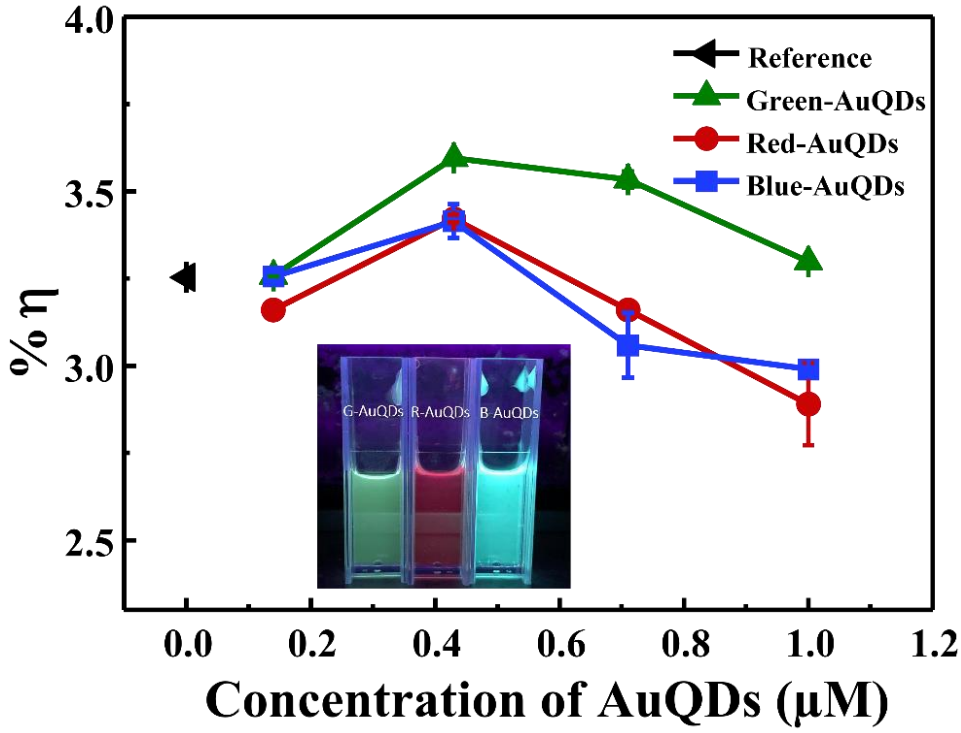

Figure 3.1 The solar cell efficiency (%η) of the AuQDs-incorporated inverted OSCs as a function of AuQDs concentration, compared with the reference cell. (Inset is the photographs of AuQD solutions under 365 nm UV radiation).

In addition, 0.43 μM of G-AuQDs absorb UV light which show absorption spectra at wavelength below 450 nm and emit fluorescence (visible light) at the wavelength of around 510 nm [27, 30], which overlaps with the absorption of the photoactive region. Normally, the photoelectric conversion and absorption properties of the P3HT:PCBM have weak absorption in region of the UV. Therefore, G-AuQDs are used as photosensitizer to harvest UV radiation from the sunlight and convert to visible light into the photoactive film for improving the inverted OSC performance. Moreover, the fluorescence intensity of G-AuQDs-incorporated PEDOT:PSS layers is studied. The starting AuQDs are in water. For device fabrication, AuQDs are mixed with PEDOT:PSS matrix due to water solubility. The result shows that the fluorescence and absorption spectra of G-AuQDs remain almost the same. From figure 3.2a, intensity of fluorescence is lowered resulting from the presence of PEDOT:PSS in the solution.

G-AuQDs exhibit strong fluorescence intensity (510 nm) while PEDOT:PSS can adsorb a wide range of light in visible and near-infrared (NIR) region, as shown in the Figure 3.2b. After G-AuQDs are embedded into the PEDOT:PSS matrix, the fluorescence intensity decreases, as compared with that of only G-AuQDs at the same concentration due to masking by PEDOT:PSS matrix. We found that the HTL particles surrounding the G-AuQDs offer fluorescence light for other components in the cell, especially P3HT:PCBM film. Therefore, the fluorescence of AuQDs embedded into the PEDOT:PSS matrix can be absorbed within the active molecules of the solar cell device, leading to enhanced PCE. This agrees well with the invested OSCs performances, which are listed in Table 1.

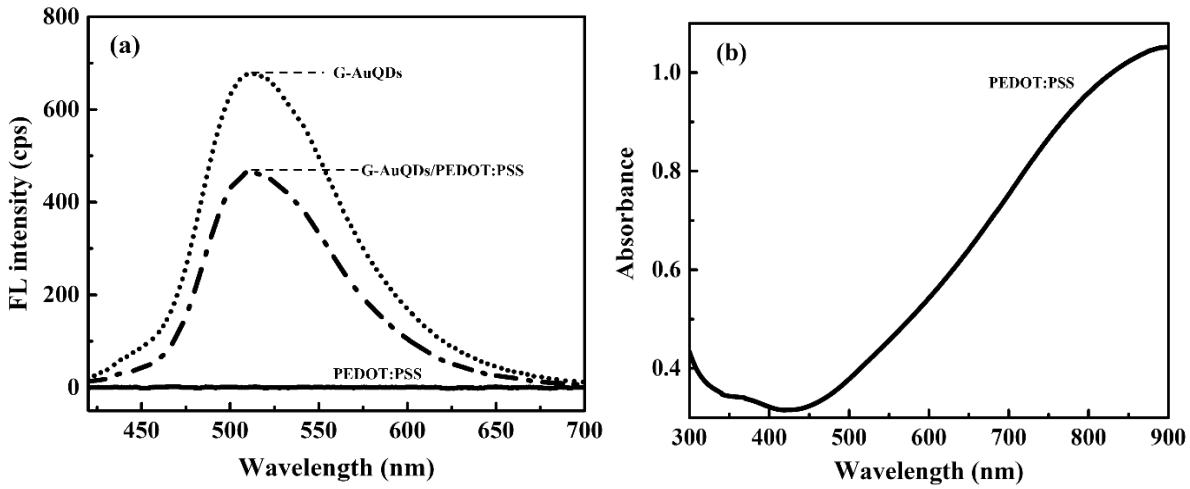

Figure 3.2 (a) The fluorescence spectra of G-AuQDs, G-AuQDs/PEDOT:PSS, and PEDOT:PSS aqueous solutions and (b) UV-vis absorption of PEDOT:PSS aqueous solutions.

Table 3.1 Photovoltaic parameters of the incorporating AuQDs into the invested OSCs.

Devices	Parameters				
	J_{sc} (mA/cm^2)	V_{OC} (V)	FF (%)	η (%)	Enhancement (%)
Reference inverted OSCs	6.88±0.10	0.64	0.55	3.25±0.01	-
G-AuQDs-loaded inverted OSCs	7.29±0.03	0.65	0.57	3.60±0.01	10.77
R-AuQDs-loaded inverted OSCs	6.90±0.02	0.64	0.58	3.42±0.01	5.23
B-AuQDs-loaded inverted OSCs	7.18±0.08	0.64	0.56	3.41±0.05	4.92

To investigate the photovoltaic properties, we measured the *J-V* characteristics of our developed inverted OSCs. The photovoltaic parameters and *J-V* characteristics of the inverted OSCs loaded with the 0.43 µM of AuQDs and a reference cell are illustrated in Table 1 and Figure 3.3, respectively. The reference cell without AuQDs exhibits a J_{sc} of 6.88 mA/cm^2, a V_{oc} of 0.64 V, an FF of 0.55, and a PCE value of 3.25%. In all inverted OSC devices loaded the different AuQDs types, the values of the photocurrent are higher than that of the reference cell. The J_{sc} values are 7.29, 6.90, and 7.18 mA/cm^2 for the G- AuQDs, R-AuQDs and B-AuQDs inverted OSC devices, respectively. The PCE values are found to be increased when incorporating AuQDs into the devices, representing 3.60% PCE (10.77% enhancement), 3.42% PCE (5.23% enhancement), and 3.41% PCE (4.92% enhancement) for the G- AuQDs, R- AuQDs, and B-AuQDs incorporated devices, respectively, whilst insignificant change in V_{oc} for all cells is observed. These enhancements imply that AuQDs act as photoactive layer to harvest visible light and photosensitizers to absorb photons in near UV and UV regions, leading to the enhanced broadband light absorption [46, 47]. Meanwhile, the improvement in efficiency can be achieved from the plasmonic effect due to the aggregation of AuQDs (AuNPs-like NPs) [27]. All of the possible effects through introducing the AuQDs into the solar cells can

contribute to the enhancement of their device performances. In comparing three types of AuQDs-based solar cells, we observe that the conversion efficiency enhancement of G-AuQDs, which are introduced in the HTL layer of the devices, is higher than those of both the R- AuQDs and B-AuQDs-based devices because the strong fluorescence emission of G-AuQDs correlates with the absorption wavelength of photoactive compounds, suggesting additional fluorescence harvesting as observed with the highest *Jsc* value. Therefore, incorporating the G-AuQDs in the cells provides a remarkable enhancement. In comparison to conventional OSC device incorporated AuQDs, it is found that the PCE value of the inverted OSCs containing G-AuQDs in the HTL (10.77% enhancement) is higher than of previously reported conventional OSCs structure (8.26% enhancement) [30, 31]. This is because the fluorescent light occurred near the Ag surface can also be attributed to the enhanced photocarrier generation in the photoactive material.

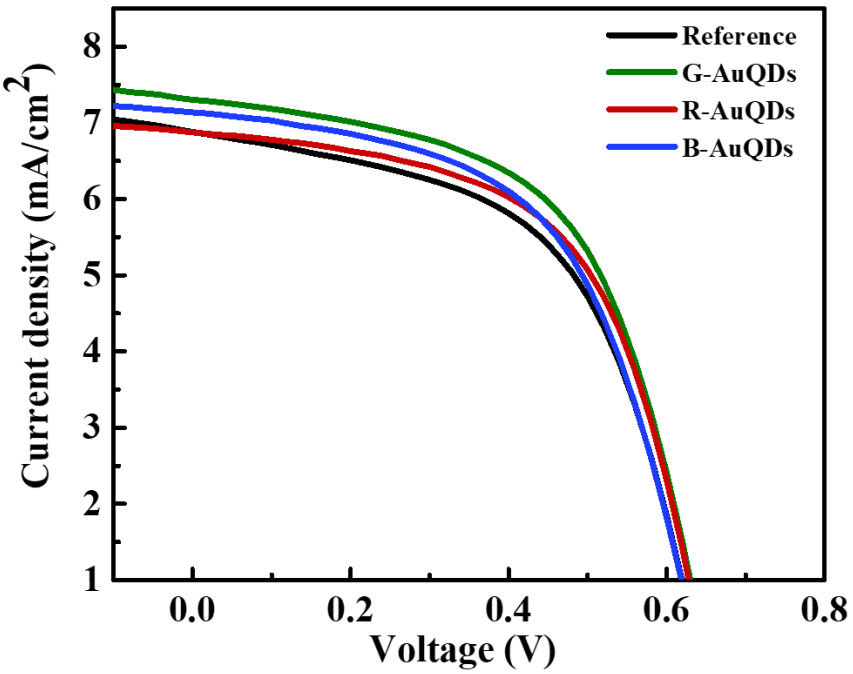

Figure 3.3 *J-V* characteristics of the AuQDs-incorporated inverted OSCs in comparison to the reference cell without metal AuQDs.

3.2 Optical property-surface morphology of the developed inverted OSCs

The optical properties of developed inverted OSCs are investigated in order to confirm the GCSPR excitation of the DVD-R and BD-R metal grating electrodes, as illustrated in Figure 3.4. For flat inverted OSC, the sharp SPR peak is not appeared over all incident angles, which has a similar pattern for whole wavelength scan (Figure 3.4a). The broadband low-reflectivity peak in the range of 400-650 nm indicates light absorption by the photoactive material of the inverted OSC. The reflection spectra for the inverted OSCs based on DVD-R and BD-R Ag grating electrodes are observed with the sharp SPR peaks at many different incident light angles (20° to 60°) by illumination with *p*-polarized (*p*-pol) light, as seen in Figures 3.4b and 3.4c, respectively. The reflectivity of the DVD-R grating is broader than those of both the flat cell and BD-R grating because of the light scattering (weak SPR property), which leads to an increase absorption ability of the photoactive material. Especially, we observed a dip peak at wavelengths 400-600 nm in DVD-R grating. The dip wavelength depends on the angle of incidence, which indicates GCSPR property on the metal grating electrode. Additionally, the reflectivity of the flat device (reflectivity below 0.1) is longer than the DVD-R grating (reflectivity value of 0.15) at 520 nm, but the DVD-R grating shows broader range of lowering reflectivity. Due to the fact that photoactive material (P3HT:PCBM) absorbs the light in broad wavelength, the broader reflectivity lowered by DVD-R grating can lead to the increase in PCE. Furthermore, an additional optical absorption from GCSPR/waveguide mode (650-800 nm) is found in the BD-R and DVD-R metallic nanogratings [48]. The results confirm that the GCSPR on grating structure can be excited by a *p-pol* light irradiation. For comparisons of two grating height between the DVD-R and BD-R devices, deeper SPR dip peaks are obtained for the DVD-R grating since the DVD-R pattern has higher grating height than the BD-R pattern. As known that GCSPR can improve the performances of solar cells [49], it is expected that grating can improve more additional light harvesting to the OSCs based G-AuQDs.

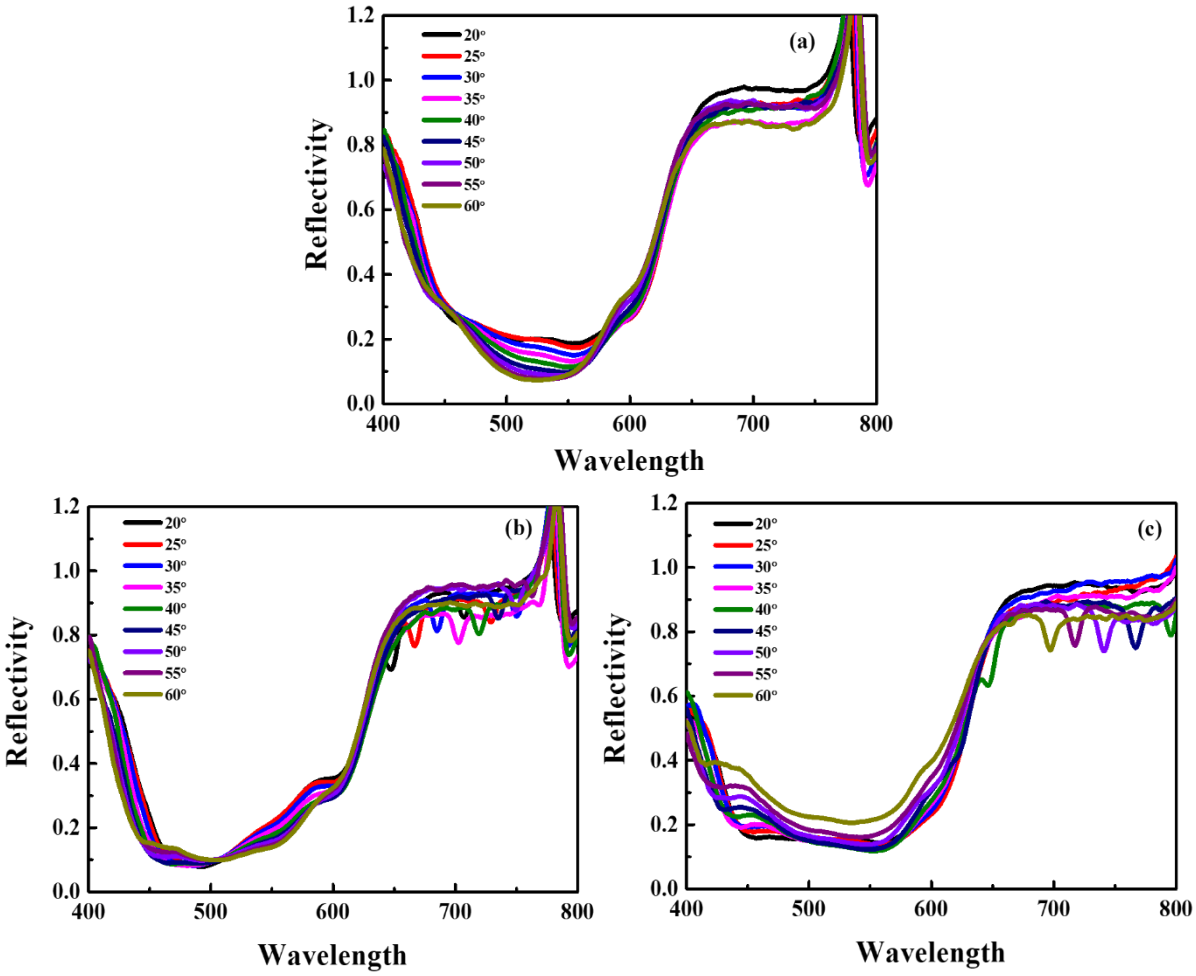

Figure 3.4 The SPR reflectivity curves of (a) bare cell (b) G-AuQDs/BD-R and (c) G-AuQDs/DVD-R grating of inverted OSCs irradiated with *p*-polarization [50].

The surface morphology of the thin films is studied by AFM measurements. The AFM images of the fabricated inverted OSC components are shown in Figure 3.5. For comparison, the roughness of the ITO film (4.98 nm) is larger than that of the TiO_2/ITO film (4.65 nm) as shown in Figures 3.5a and 3.5b, respectively. It can be clearly seen that the TiO_2 film has been deposited onto the ITO surface, leading to a smooth surface morphology. Figures 3.5c and 3.5d show AFM images of the BD-R and DVD-R grating nanostructures of the active layer, indicating that the nanopatterns obtained from diffraction gratings are perfectly moved from the master templates to the surfaces of photoactive layer. The both nanopatterns on the films are of one-dimensional grating structures and the grating height of the BD-R pattern (10 nm)

is smaller than that of the DVD-R pattern (31 nm), as seen in Figure 3.6. After coating with HTL and then depositing Ag electrode, the device structure is expected to obtain the metallic Ag grating electrode. This is confirmed with the reflectivity dip peaks for both kinds of the inverted OSCs at the high wavelength region as observed in Figures 3.4b and 3.4c.

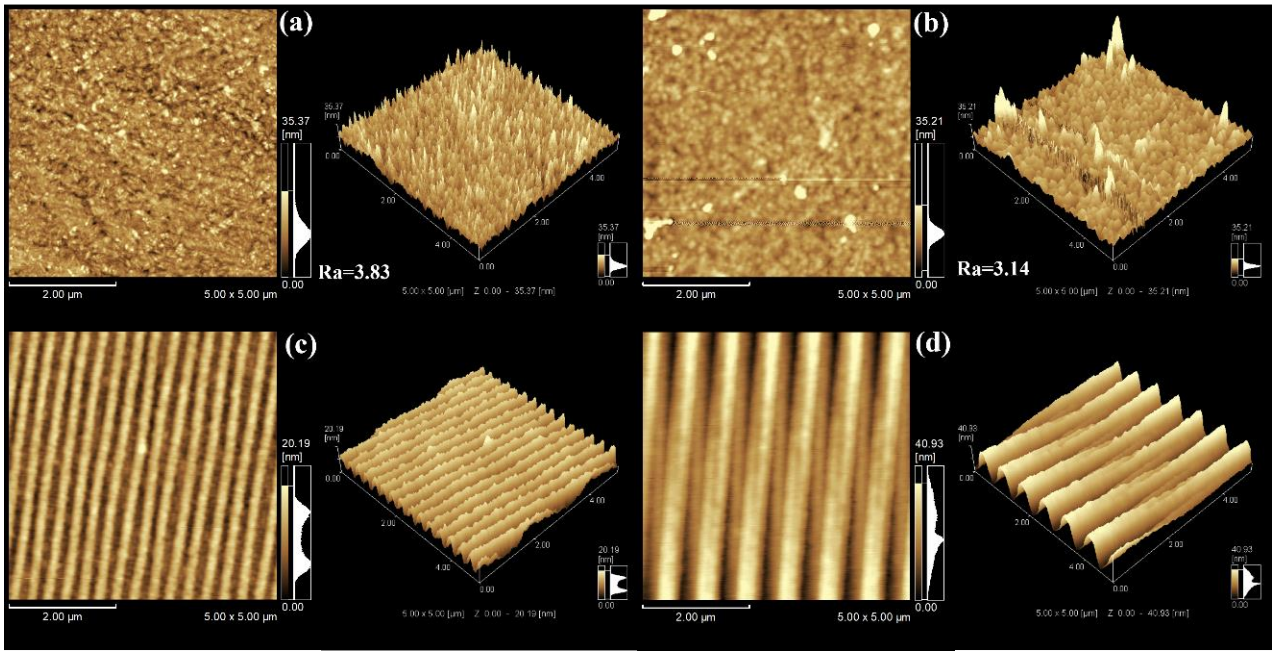

Figure 3.5 Surface morphology of (a) bare ITO, (b) TiO_2 film, and the P3HT:PCBM film imprinting of (c) BD-R and (d) DVD-R grating patterns.

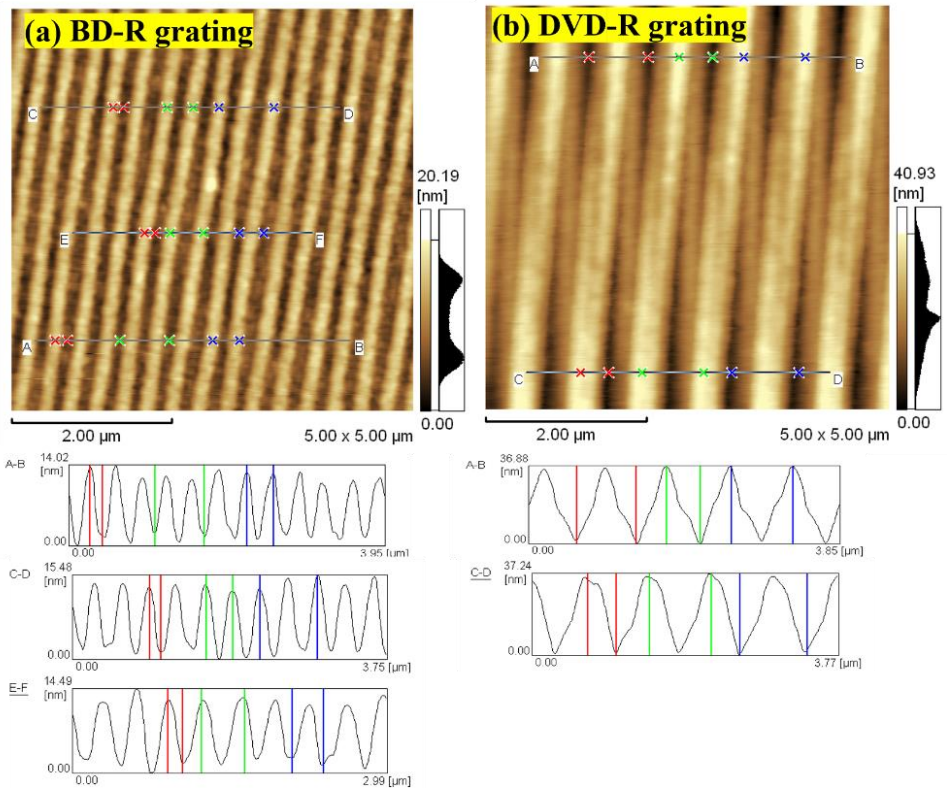

Figure 3.6 The AFM line profiles of the P3HT:PCBM film imprinting of (a) BD-R and (b) DVD-R grating structure.

3.3 Photovoltaic performances of G-AuQDs/grating structure

The influence of the introducing additional grating structures into the inverted OSCs are investigated. The *J-V* properties of the BD-R and DVD-R grating structures in fabricated inverted OSC device are shown in Figure 3.7, and electrical parameters are listed in Table 2. Both BD-R and DVD-R patterns are created for fabrication of Ag grating top electrodes on the inverted OSCs as explained above. The results demonstrate that both BD-R and DVD-R patterns are higher photovoltaic performances than that of flat reference cell. The *Jsc* values are 7.24 and 7.14 mA/cm^2 for the DVD-R and BD-R grating-based inverted OSCs, respectively. The DVD-R and BD-R grating incorporated into devices result in the enhanced PCE of 3.50% (7.69% enhancement) and 3.48% (7.08% enhancement) and there is little change in the FF and *Voc*. These enhancements are due to the results that the grating structure provide

both light scattering and the GCSPR effect, offering the improvement in performances of the inverted OSCs [48]. The efficiency enhancement of the DVD-R grating is better than the BD-R grating. This is caused by stronger light scattering and GCSPR excitation. A difference in grating height may result in a difference in the power conversion efficiency. Compared to previous study, it is found that the efficiency of the conventional OSCs based on plasmonic grating (10.40% enhancement for BD-R) [31] is higher than that of our developed inverted OSC (7.08% enhancement for BD-R). In the inverted structure of OSCs, the HTL (PEDOT:PSS) is formed in between the active layer and Ag grating layers, resulting in the weaker GCSP excitation. Besides, the insertion of TiO_2 interlayer in the inverted OSC device results in the lower grating height than previously studied in the conventional OSCs, leading to the weak GCSPR excitation (see Figure 3.4).

After studying the effect of only introduction of AuQD or only metallic grating into inverted OSC device, we investigate the effects of a combination of AuQDs with metallic grating into the inverted OSCs for improvement the properties of photovoltaic devices. The results from this study clearly indicate that blending the G-AuQDs in the HTL layer show the greatest efficiency when compared to B-and R-AuQDs, as illustrated in Figures 3.1 and 3.3. At the same conditions, G-AuQDs are embedded into HTL for boosting light harvesting, and diffraction grating patterns were fabricated on the P3HT:PCBM layer surface as well as on Ag top electrode by the nanoimprinting technique for photon trapping and generation of GCSPR excitation [48]. Figure 3.7 compare the *J-V* properties of different G-AuQDs/grating structures and electrical parameters of the developed OSCs are listed in Table 2. When the G-AuQDs and/or plasmonic grating structure (BD-R or DVD-R pattern) are introduced to the devices, the *Jsc* values increase from 7.14 (BD-R) to 7.57 mA cm^{-2} (BD-R/G-AuQDs), and 7.24 (DVD-R) to 7.75 mA cm^{-2} (DVD-R/G-AuQDs), and the PCE values enhance from 7.08% (BD-R) to 13.85% (BD-R/G-AuQDs) and 7.69% (DVD-R) to 16.0% (DVD-R/G-AuQDs) while no

significant change is observed in *Voc* and the FF. As a result, we found that the incorporation of G-AuQDs with grating structure exhibits better device performance than the device with individual G-AuQDs or individual grating structure because it presents synergistic effect in the inverted OSC system that has benefit in light management. The result suggests that in each G-AuQD/grating system exhibit synergistic enhancement. The improvement of the G-AuQD/BD-R grating (η = 3.70%) is found to be 6.3% compared to BD-R grating (η = 3.48%) For G-AuQD/DVD-R grating (η = 3.77%), it is found to be 7.7% compared to DVD-R grating (η = 3.50%). In the hybrid systems, the greatest PCE and *Jsc* values of developed device are observed in the combination of G-AuQDs and DVD-R grating structure that agree with individual DVD-R grating pattern, which offers better increase in both values as compared with those of individual BD-R grating pattern. Hence, the results above suggest that the device containing G-AuQDs with DVD-R grating system exhibits the greatest synergistic effect.

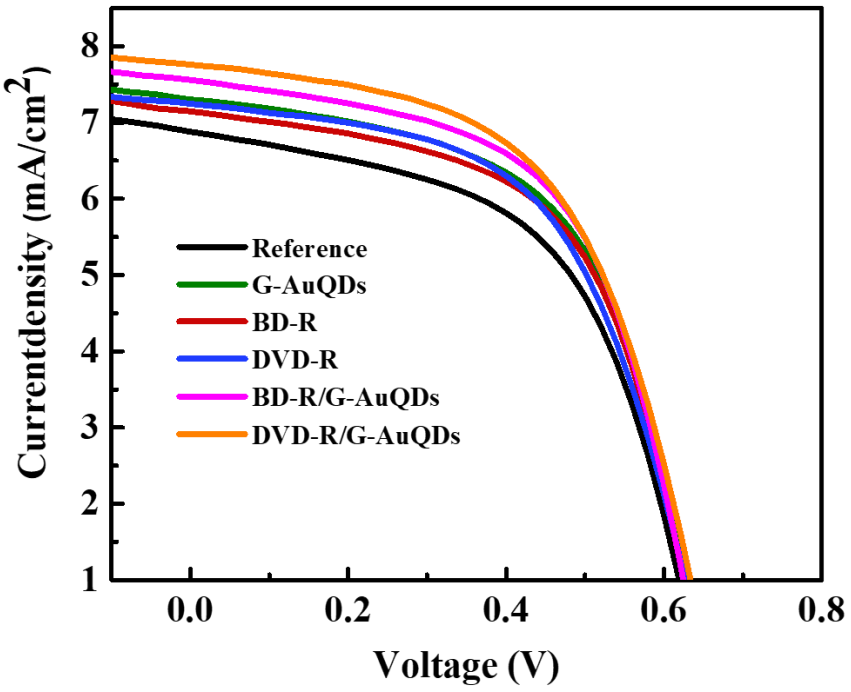

Figure 3.7 *J-V* characteristics of the G-AuQDs and/or plasmonic grating structures inverted OSCs in comparison to the reference cell.

Table 3.2 The electrical parameters of different inverted OSCs structures.

Devices	Parameters				
	J_{sc} (mA/cm^{-2})	V_{OC} (V)	FF (%)	η (%)	Enhancement (%)
Reference	6.88±0.10	0.63	0.55	3.25±0.01	-
G-AuQDs	7.29±0.03	0.65	0.57	3.60±0.01	10.77
BD-R	7.14±0.14	0.64	0.57	3.48±0.05	7.08
DVD-R	7.24±0.01	0.65	0.56	3.50±0.01	7.69
BD-R/G-AuQDs	7.57±0.01	0.64	0.58	3.70±0.03	13.85
DVD-R/G-AuQDs	7.75±0.03	0.65	0.56	3.77±0.01	16.00

To further elucidate the effect of G-AuQDs/grating structure-based inverted OSCs, the IPCE (incident photon-to-current efficiency) and E.F. (IPCE enhancement factors) are measured in a wavelength range of 300 to 800 nm, as shown in Figures 3.8A and 3.8B, respectively. The inverted OSC device loaded with only G-AuQDs or only grating system show greater IPCE values and broader wavelength range than those of the flat cell. After loading both G-AuQDs and metallic grating in the devices, the IPCE value is higher than individual systems. Additionally, we plotted the E.F. profile (the ratio of the IPCE values of the developed cells to the flat cell), as seen in Figures 3.8B. It is found that the enhancement of IPCE over the full wavelength range (300-800 nm) is observed for all the developed devices. For the G-AuQDs in inverted OSC, the enhanced IPCE is observed in the range of 380-450 nm, which is caused by light harvesting thought utilization of G-AuQDs in inverted OSC [27, 30]. Interestingly, the highest improvement is found for the device containing G-AuQDs with Ag grating electrode. It is noted that incident light is greatly converted into fluorescence emission by G-AuQDs together with the GCSPR excitation [30, 48]. Such higher intensity fluorescence closely matches an absorption of P3HT:PCBM photoactive layer, resulting in the best increase of E.F. in this range. Significantly, enhanced IPCE can be observed for all cases, which well correlates with its *J-V* characteristics. Moreover, the incorporations with single and dual

systems can improve the developed device over the wavelength range of 400-800 nm, which the improvement patterns of all cells over this wavelength range are similar and the smallest enhancement in the wavelength regions of 400-470 and 600-800 nm is observed for the device incorporated with G-AuQDs. All solar cells based on single and dual incorporations except a dual G-AuQDs/DVD-R Ag grating structure reveal the same E.F pattern in a wavelength region of 470-600 nm while the dual G-AuQDs/DVD-R Ag grating structure reveals higher values over this range. The devices based on both single and dual systems except a single G-AuQDs device show the insignificantly different enhanced E.F. over the range of 400-470 nm. Moreover, over the wavelength range of 600-800 nm, the cells with Ag gratings clearly give the better IPCE improvement than that of the cell with adding G-AuQDs, indicating GCSPR effect, whilst the combination of G-AuQDs and each Ag grating introduced into the inverted OSCs offers the best improvement of the IPCE value over all the cells. This would be of synergistic effect of both components, involving the UV-region light harvesting of G-AuQDs and the GCSPR excitation of Ag gratings [27, 28]. Furthermore, in this range, it is seen that the cell employing G-AuQDs/DVD-R Ag grating reveals better light harvesting than the using G-AuQDs/BD-R Ag grating system. The result of IPCE improvement by the presence of the SPR excitation over the wavelength region of 600-800 nm for both cases indicate the plasmon-enhanced fluorescence effect, namely GCSPR-enhanced fluorescence [51, 52] as observed with the best *Jsc* and PCE together with highly enhanced IPCE over a whole wavelength scan. Therefore, the more increase in the fluorescence intensity by the SPR effect gives higher consumable light intensity inside the OSC, possessing a better improvement in the light harvesting or PCE. As a result, the best light harvesting is allowed with extended light utilization in near-UV region, light trapping, GCSPR excitation, and SPR-enhanced fluorescence. Our observation suggests that the combination of G-AuQDs and DVD-R grating has the potential to enhance the photoelectric properties.

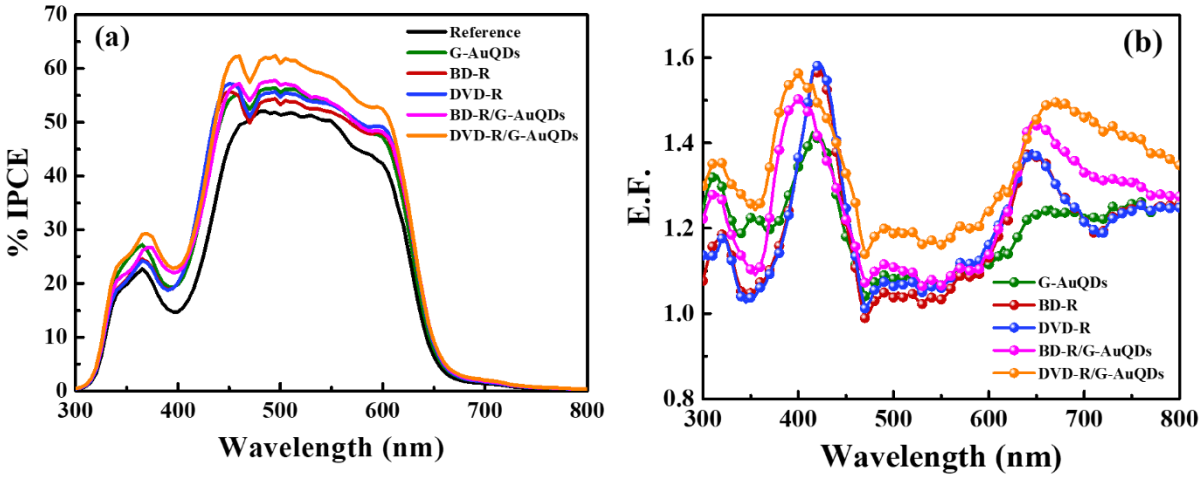

Figure 3.8 (a) IPCE spectra and (b) E.F. profiles of developed inverted OSCs [50].

3.4 The fluorescence and GCSPR properties of the G-AuQDs/grating structure

In the further study, the fluorescence emission enhancement of the G-AuQDs within GCSPR evanescent field on the plasmonic Ag grating electrode are studied (Figure 3.9). The result shows that the significant enhancement in the fluorescence emission of G-AuQDs is observed in the G-AuQDs on DVD-R Ag grating when employing the incident light angles that creates the GCSPR behavior. The SPR dip wavelength overlaps with the absorption range of the G-AuQDs at the incident light angles above 30º, resulting in a considerable increase in fluorescence intensity (Figure 3.9). It is found that the enhanced fluorescence reaches a maximum value at the incident light angle of 40º and then remains constant. Figure 3.10a shows broadband low-reflectivity in wide range of wavelengths, which indicates GCSPR excitation and light scattering on the surface, leading to the enhanced fluorescence of G-AuQD. In the case of G-AuQDs on BD-R Ag grating, an increased fluorescence intensity is observed at incident light angle of 30º at wavelength around 520 nm (Figure 3.10b) that G-AuQDs generate strong fluorescence emission in this region. At the incident light angles above 40º, the rest angles give the same fluorescence intensity with G-AuQDs on a flat Ag platform. This is due to that the SPR dip wavelength did not match with an absorption or light utilization range intensity of G-AuQDs (Figures 3.9). Thus, the GCSPR can efficiently enhance the fluorescence

of G-AuQDs when these materials are located within the GCSPR evanescent field [53] as found in the cells fabricated with G-AuQDs/DVD-R Ag grating. The evidence above suggests that the G-AuQDs/BD-R Ag grating presents the significantly low level of GCSPR-enhanced florescence for our developed inverted OSC, which its non-synergic improvement is of individual contributions from the light harvesting of G-AuQDs and light trapping and scattering by GCSPR behavior. The higher PCE improvement in the G-AuQDs/DVD-R nanopatterned Ag grating system-based inverted OSC is from the GCSPR-enhanced florescence effect. This agrees well with the photovoltaic study that the G-AuQDs/DVD-R patterned Ag grating electrode gives the excellent improvement in the solar cell performances.

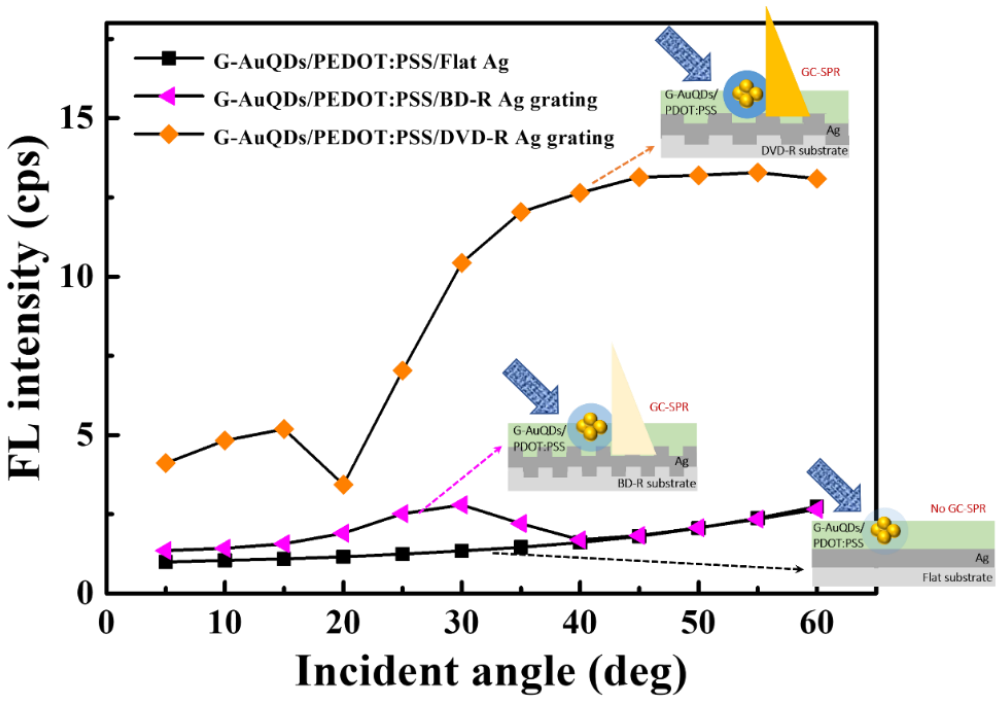

Figure 3.9 Fluorescence enhancement spectra of G-AuQDs/PEDOT:PSS film deposited on Ag-coated on flat, BD-R and DVD-R gratings substrates [50].

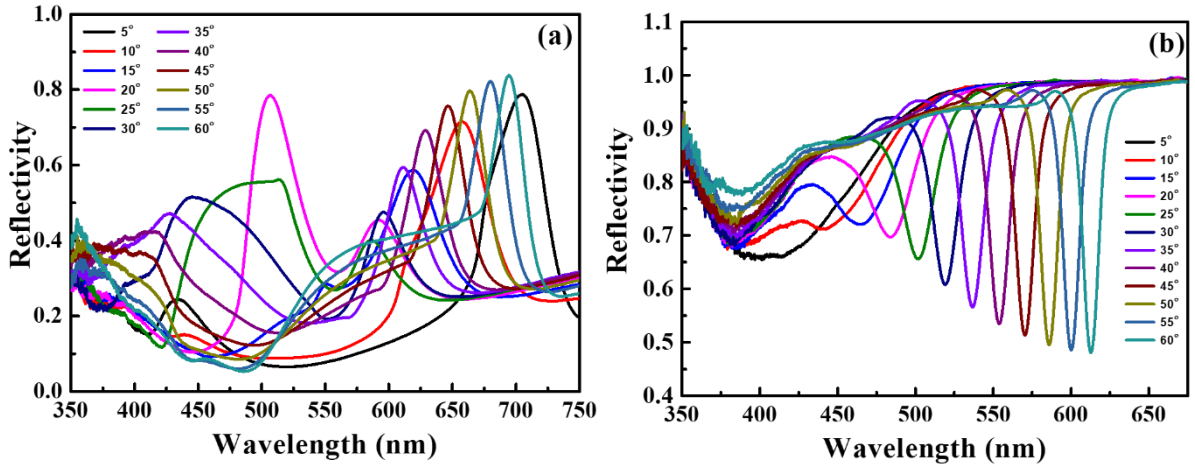

Figure 3.10 SPR curves of AuQDs/PEDOT:PSS coated on (a) DVD-R Ag- and (b) BD-R Ag-grating substrate [50].

3.5 Electrochemical impedance spectroscopy of the developed inverted OSCs

The interfacial properties of the inverted OSCs were investigated by electrochemical impedance spectroscopy (EIS). Table 3 illustrates the resistance (R_s and R_{ct}) values for all developed devices. The Nyquist diagrams from the electrochemical impedance data of the AuQD-incorporated devices and the reference cell under illumination by solar light are presented in Figure 3.11a. We found that the AuQD-incorporated devices exhibit smaller R_s values than the control device. The resistance of developed cell decreases due to adding AuQDs in the device. The R_{ct} values are 9.9, 8.5, 8.7 and 9.6 Ω for the reference, G-, R and B-AuQDs, respectively. The R_{ct} value is decreased in the case of AuQD-incorporated devices because the loading AuQDs into HTL layer can enhance the charge transfer properties [30, 54]. Meanwhile, excited electrons of the AuQDs at the interface between the PEDOT:PSS/AuQDs blend film and P3HT:PCBM active layer can be jumped into the conduction band of the acceptor, which also increase short-circuit currents of the devices [27]. Moreover, the incorporating with AuQDs might improve the surface roughness of PEDOT:PSS film, which reduces a contact resistance at the photoactive layer/HTL interface. The decreases in both R_s and R_{ct} values of such AuQDs devices are due to the good interfacial contact and improve the electric mobility

as well as the performance of the devices. It is noted that among all, G-AuQDs offers the best interface between the film components as agreed with our study of the photovoltaic properties of the device.

When the G-AuQDs and grating structure are introduced to the devices, the R_s values of G-AuQDs and G-AuQD/Ag gratings are smaller and R_s of the grating structure cell is slightly lower, than that of the flat cell. This indicates that the interfacial contact resistances of the fabricated cells are greatly decreased due to combining G-AuQDs and metallic grating electrode into the devices as shown in Figure 3.11b. Furthermore, as compared to the individual cells and a reference, the decreased R_{ct} value of the fabricated solar cell is also observed, owing to effect of incorporation of the G-AuQDs and grating structure Ag film into devices. The reference cell has the R_{ct} value of 9.9 Ω while the inverted OSCs fabricated with G-AuQD, BD-R grating, DVD-R grating, G-AuQD/BD-R grating, and G-AuQD/DVD-R grating show low R_{ct} values of 8.5, 8.6, 8.8, 7.9 and 7.7 Ω, respectively. Thus, adding both G-AuQDs and grating structure into the devices can enhance the charge transfer resistance the devices, as seen with the lowest R_{ct}. This is due to the best interface of each component and improved electric conductivity. The EIS result for the G-AuQDs/DVD-R grating system well agrees with its J_{sc} and PCE.

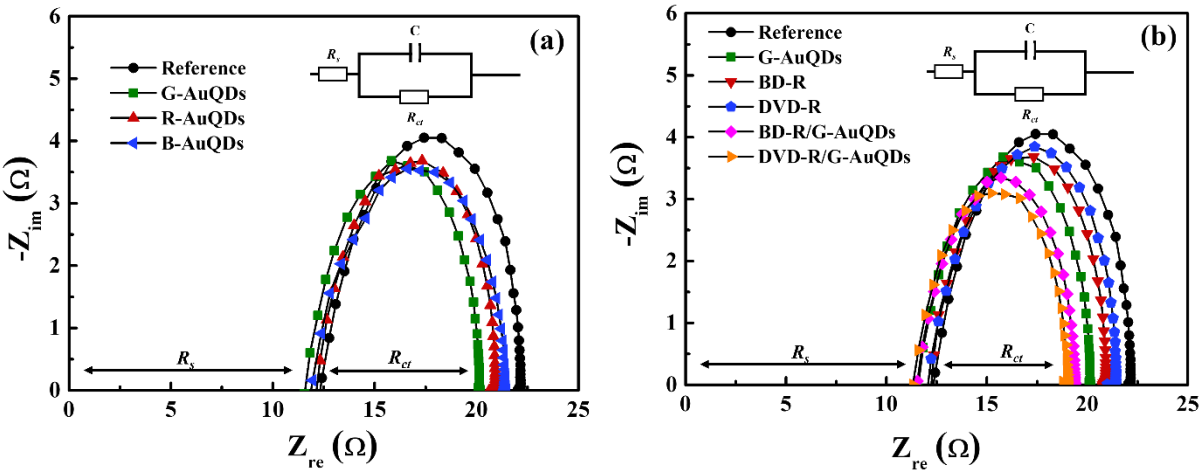

Figure 3.11 Nyquist plots of the inverted OSCs based on (a) individual AuQDs and (b) the G-AuQDs and/or plasmonic grating structures as compared to that of the bare cell [50].

Table 3.3 Resistance values and average electron lifetimes (τ_{avg}) and maximum frequencies (f_{max}) of fabricated inverted OSCs.

Devices	**Parameters**			
	R_s **(Ω)**	R_{ct} **(Ω)**	τ_{avg}	f_{max} **(kHz)**
Reference	12.4	9.9	4.48	35.48
G-AuQDs	11.6	8.5	3.56	44.67
R-AuQDs	12.3	8.7	4.00	39.81
B-AuQDs	11.9	9.6	4.00	39.81
BD-R	12.2	8.6	4.00	39.81
DVD-R	12.1	8.8	4.00	39.81
BD-R/G-AuQDs	11.5	7.9	4.00	39.81
DVD-R/G-AuQDs	11.3	7.7	3.56	44.67

In addition, the frequency peaks of all developed OSCs in the Bode phase plots, which is associated with the electron lifetime [30, 55] are shown in Figure 3.12. The average electron lifetime (τavg) values are summarized in Table 3. It is found that the τavg values of all devices are insignificantly difference. This result clearly indicates that utilizing AuQDs, grating structure, or both systems may not affect the lifetime of electron. Thus, the modification of the inverted OSC configuration with single and dual systems improves the device performances by the enhanced photocarrier generation due to UV and near-UV light harvesting of AuQDs, light trapping and scattering, and/or GCSPR excitation, rather than from the extended carrier lifetime in device. For G-AuQDs/Ag grating-based inverted OSCs, the excellent photocarrier generation is due to the synergistic effect of G-AuQDs and Ag grating through the behavior of GCSPR-enhanced fluorescence emission.

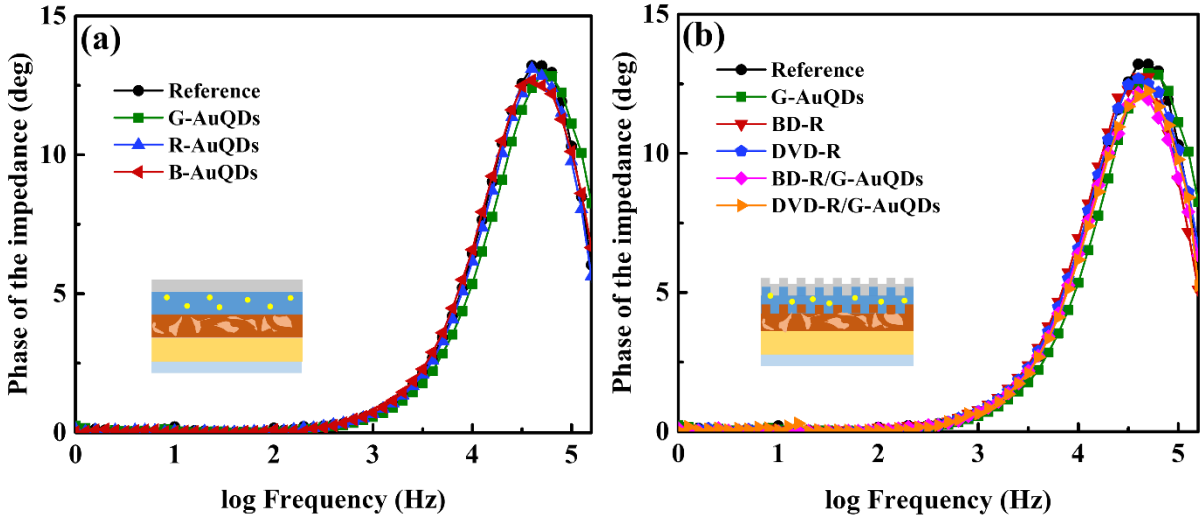

Figure 3.12 Bode phase plots of the inverted OSCs based on (a) individual AuQDs systems and (b) the G-AuQDs and/or plasmonic grating structures (in comparison with the reference cell).

CHAPTER 4

Conclusion

In summaries, we have successfully developed the new inverted OSC using the AuQDs blended in the hole transport layer and grating-structured Ag top electrode. This system can enhance light harvesting, which increases the performance of the inverted OSC. The effect of three kinds of AuQDs with different emission wavelengths, including B-AuQDs, G-AuQDs, and R-AuQDs, in the inverted OSCs are investigated. All types of AuQDs show significant improvement of efficiency compared with that of flat reference cell. The G-AuQDs offer the best device performance of the inverted OSCs. Two different types of diffraction grating, DVD-R and BD-R, are used as master templates to construct metallic grating top electrodes onto the P3HT:PCBM layer surface. To better improve the solar cell efficiency, combining both AuQDs and GCSPR into inverted OSCs is demonstrated. The synergistic effect between the two system is observed, and the efficiency enhancement from fluorescence of G-AuQDs surrounded by the GCSPR evanescent field on the metal grating surface is found. The higher *Jsc* and PCE values of the developed device involve the multiple effects such as light harvesting by AuQDs-emitted fluorescence, scattering inside the cell by plasmonic grating structures (GCSPR effect), AuQD fluorescence-induced additional GCSPR emission and the GCSPR-enhanced fluorescence effect. The synergistic effects of G-AuQDs and GCSPR are obtained because the GCSPR excitation wavelength at the metallic grating gives a closely match for the absorption range of the AuQDs, thus leading to an enhancement. The proposed inverted OSC consisting of G-AuQD and DVD-R Ag grating electrodes offers a *Jsc* value of 7.75 mA/cm^2 and a PCE value up to 3.77% (16% enhancement). Our strategy is an alternative approach for

enhancing the device performances and it has the potential to develop other kinds of the solar cells.

REFERENCES

[1] M. Zerta, P. R.Schmidt, C. Stiller, and H. Landinger, Alternative world energy outlook (AWEO) and the role of hydrogen in a changing energy landscape, *International Journal of Hydrogen Energy* **33** (2008) 3021-3025.

[2] T. Ahmad, and D. Zhang, A critical review of comparative global historical energy consumption and future demand: The story told so far, *Energy Reports* **6** (2020) 1973-1991.

[3] E. R. Rwenyagila, A review of organic photovoltaic energy source and its technological designs, *International Journal of Photoenergy* **2017** (2017), 1656512.

[4] J. Weickert, R. B. Dunbar, H. C. Hesse, W. Wiedemann, and L. Schmidt-Mende, Nanostructured organic and hybrid solar cells, *Advanced Materials* **23** (2011) 1810-1828.

[5] U.S. energy information administration, Monthly energy review, Table 1.3 and 10.1. preliminary data (2021).

[6] N. Edomah, Economics of energy supply, In reference module in earth systems and environmental sciences, *Elsevier* (2018).

[7] A. Peter Amalathas, and M. M. Alkaisi, Nanostructures for light trapping in thin film solar cells, **10** (2019) 619.

[8] H. Heidarzadeh, A. Rostami, S. Matloub, M. Dolatyari, and G. Rostami, Analysis of the light trapping effect on the performance of silicon-based solar cells: Absorption enhancement, *Applied Optics* **54** (2015) 3591-3601.

[9] D. M. Chapin, C. S. Fuller, and G. L. Pearson, A new silicon p-n junction photocell for converting solar radiation into electrical power, **25** (1954) 676-677.

[10] April 25, 1954: Bell laboratories demonstrates the first practical silicon solar cell, APS News, American Physical Society **18** (2009).

[11] H. Spanggaard, and F. C. Krebs, A brief history of the development of organic and polymeric photovoltaics, *Solar Energy Materials and Solar Cells* **83** (2004) 125-146.

[12] K. Orgil, Comparison of organic and inorganic solar photovoltaic systems, San Luis Obispo, California Polytechnic State University (2018).

[13] I. Arbouch, Y. Karzazi, and B. Hammouti, Organic photovoltaic cells: Operating principles, recent developments and current challenges - review, *Physical and Chemical News* **72** (2014) 73-84.

[14] A. M. J. I. J. O. L. Bagher, and Arts. Comparison of organic solar cells and inorganic solar cells **3** (2014) 53.

[15] S. Dai, S. Chandrabose, J. Xin, T. Li, K. Chen, P. Xue, K. Liu, K. Zhou, W. Ma, J. M. Hodgkiss, and X. Zhan, High-performance organic solar cells based on polymer donor/small molecule donor/nonfullerene acceptor ternary blends, *Journal of Materials Chemistry A* **7** (2019) 2268-2274.

[16] K. He, P. Kumar, Y. Yuan, and Y. Li, Wide bandgap polymer donors for high efficiency non-fullerene acceptor based organic solar cells, *Materials Advances* **2** (2021) 115-145.

[17] Y.-X. Zhang, C. Gao, J.-D. Chen, W. Li, Y.-Q. Li, and J.-X. Tang, Dual-grating-induced light harvesting enhancement in organic solar cells, *Journal of Materials Chemistry A* **6** (2018) 11830-11837.

[18] F. Jin, Z. Su, B. Chu, P. Cheng, J. Wang, H. Zhao, Y. Gao, X. Yan, and W. Li, Interface engineering of organic Schottky barrier solar cells and its application in enhancing performances of planar heterojunction solar cells, *Scientific Reports* **6** (2016) 26262.

[19] M. Wang, and F. Wudl, Top-down meets bottom-up: organized donor-acceptor heterojunctions for organic solar cells, *Journal of Materials Chemistry* **22** (2012) 24297-24314.

[20] M.-E. Ragoussi, and T. Torres, New generation solar cells: concepts, trends and perspectives, *Chemical Communications* **51** (2015) 3957-3972.

[21] A. J. Heeger, 25th anniversary article: Bulk heterojunction solar cells: Understanding the mechanism of operation, *Advanced Materials* **26** (2014) 10-28.

[22] N. Yeh, and P. Yeh, Organic solar cells: Their developments and potentials, *Renewable and Sustainable Energy Reviews* **21** (2013) 421-431.

[23] G. Chidichimo, and L. Filippelli, Organic Solar Cells: Problems and Perspectives, *International Journal of Photoenergy* **2010** (2010) 123534.

[24] Z. Yin, J. Wei, and Q. Zheng, Interfacial materials for organic solar cells: Recent advances and perspectives, *Advanced Science* **3** (2016) 1500362.

[25] C. N. Hoth, S. A. Choulis, P. Schilinsky, and C. J. Brabec, High photovoltaic performance of inkjet printed polymer:fullerene blends, *Advanced Materials* **19** (2007) 3973-3978.

[26] A. Pangdam, S. Nootchanat, R. Ishikawa, K. Shinbo, K. Kato, F. Kaneko, C. Thammacharoen, S. Ekgasit, and A. Baba, Effect of urchin-like gold nanoparticles in organic thin-film solar cells, *Physical Chemistry Chemical Physics* **18** (2016) 18500-18506.

[27] A. Pangdam, S. Nootchanat, C. Lertvachirapaiboon, R. Ishikawa, K. Shinbo, K. Kato, F. Kaneko, S. Ekgasit, and A. Baba, Investigation of gold quantum dot enhanced organic thin film solar cells, *Particle and Particle Systems Characterization* **34** (2017) 1-8.

[28] S. Nootchanat, A. Pangdam, R. Ishikawa, K. Wongravee, K. Shinbo, K. Kato, F. Kaneko, S. Ekgasit, and A. Baba, Grating-coupled surface plasmon resonance enhanced organic photovoltaic devices induced by Blu-ray disc recordable and Blu-ray disc grating structures, *Nanoscale* **9** (2017) 4963-4971.

[29] T. Putnin, C. Lertvachirapaiboon, R. Ishikawa, K. Shinbo, K. Kato, S. Ekgasit, K. Ounnunkad, and A. Baba, Enhanced organic solar cell performance: Multiple surface

plasmon resonance and incorporation of silver nanodisks into a grating-structure electrode, *Opto-Electronic Advances* **2** (2019) 190010.

[30] S. Phetsang, A. Phengdaam, C. Lertvachirapaiboon, R. Ishikawa, K. Shinbo, K. Kato, P. Mungkornasawakul, K. Ounnunkad, and A. Baba, Investigation of a gold quantum dot/plasmonic gold nanoparticle system for improvement of organic solar cells, *Nanoscale Advances* **1** (2019) 792-798.

[31] S. Phetsang, S. Nootchanat, C. Lertvachirapaiboon, R. Ishikawa, K. Shinbo, K. Kato, P. Mungkornasawakul, K. Ounnunkad, and A. Baba, Enhancement of organic solar cell performance by incorporating gold quantum dots (AuQDs) on a plasmonic grating, *Nanoscale Advances* **2** (2020) 2950-2957.

[32] B. Qi, and J. Wang, Fill factor in organic solar cells, *Physical Chemistry Chemical Physics* **15** (2013) 8972-8982.

[33] S. Günes, H. Neugebauer, and N. S. Sariciftci, Conjugated polymer-based organic solar cells, *Chemical Reviews* **107** (2007) 1324-1338.

[34] S. Lattante, Electron and hole transport layers: Their use in inverted bulk heterojunction polymer solar cells, *Electronics* **3** (2014) 132-164.

[35] Z. Lin, J. Chang, C. Zhang, D. Chen, J. Wu, and Y. Hao, Enhanced performance and stability of polymer solar cells by in situ formed AlO_x passivation and doping, *The Journal of Physical Chemistry C* **121** (2017) 10275-10281.

[36] K. L. Kelly, E. Coronado, L. L. Zhao, and G. C. Schatz, The optical properties of metal nanoparticles: The influence of size, shape, and dielectric environment, *The Journal of Physical Chemistry B* **107** (2003) 668-677.

[37] K. A. Willets, and R. P. V. Duyne, Localized surface plasmon resonance spectroscopy and sensing, *Annual Review of Physical Chemistry* **58** (2007) 267-297.

[38] H. A. Atwater, and A. Polman, Plasmonics for improved photovoltaic devices, *Nature Materials* **9** (2010) 205-213.

[39] S. Eustis, and M. A. El-Sayed, Why gold nanoparticles are more precious than pretty gold: Noble metal surface plasmon resonance and its enhancement of the radiative and nonradiative properties of nanocrystals of different shapes, *Chemical Society Reviews* **35** (2006) 209-217.

[40] G. H. Carey, A. L. Abdelhady, Z. Ning, S. M. Thon, O. M. Bakr, and E. H. Sargent, Colloidal quantum dot solar cells, *Chemical Reviews* **115** (2015) 12732-12763.

[41] D. Sumanth Kumar, B. Jai Kumar, and H. M. Mahesh, Chapter 3 - quantum nanostructures (QDs): An Overview, *Synthesis of Inorganic Nanomaterials* (2018) 59-88.

[42] C.-M. Liu, C.-M. Chen, Y.-W. Su, S.-M. Wang, and K.-H. Wei, The dual localized surface plasmonic effects of gold nanodots and gold nanoparticles enhance the performance of bulk heterojunction polymer solar cells, *Organic Electronics* **14** (2013) 2476-2483.

[43] L. Lu, Z. Luo, T. Xu, and L. Yu, Cooperative plasmonic effect of Ag and Au nanoparticles on enhancing performance of polymer solar cells, *Nano Letters* **13** (2013) 59-64.

[44] Y.-S. Hsiao, S. Charan, F.-Y. Wu, F.-C. Chien, C.-W. Chu, P. Chen, and F.-C. Chen, Improving the light trapping efficiency of plasmonic polymer solar cells through photon management, *The Journal of Physical Chemistry C* **116** (2012) 20731-20737.

[45] H. Kawasaki, K. Hamaguchi, I. Osaka, and R. Arakawa, ph-dependent synthesis of pepsin-mediated gold nanoclusters with blue green and red fluorescent emission, *Advanced Functional Materials* **21** (2011) 3508-3515.

[46] A. Kogo, Y. Takahashi, N. Sakai, and T. Tatsuma, Gold cluster-nanoparticle diad systems for plasmonic enhancement of photosensitization, *Nanoscale* **5** (2013) 7855-7860.

[47] N. Sakai, and T. Tatsuma, Photovoltaic properties of glutathione-protected gold clusters adsorbed on TiO_2 electrodes, *Advanced Materials* 22 (2010) 3185-3188.

[48] K. Hara, C. Lertvachirapaiboon, R. Ishikawa, Y. Ohdaira, K. Shinbo, K. Kato, F. Kaneko, and A. Baba, Inverted organic solar cells enhanced by grating-coupled surface plasmons and waveguide modes, *Physical Chemistry Chemical Physics* **19** (2017) 2791-2796.

[49] A. Baba, N. Aoki, K. Shinbo, K. Kato, and F. Kaneko, Grating-coupled surface plasmon enhanced short-circuit current in organic thin-film photovoltaic cells, *ACS Applied Materials & Interfaces* **3** (2011) 2080-2084.

[50] K. Kuntamung, P. Yaiwong, C. Lertvachirapaiboon, R. Ishikawa, K. Shinbo, K. Kato, K. Ounnunkad, and A. Baba, The effect of gold quantum dots/grating-coupled surface plasmons in inverted organic solar cells, *Royal Society Open Science* **8** (2021) 210022.

[51] Y. Jiang, H.-Y. Wang, H. Wang, B.-R. Gao, Y.-W. Hao, Y. Jin, Q.-D. Chen, and H.-B. Sun, Surface plasmon enhanced fluorescence of dye molecules on metal grating films, *The Journal of Physical Chemistry C* **115** (2011) 12636-12642.

[52] A. Nicol, and W. Knoll, Characteristics of fluorescence emission excited by grating-coupled surface plasmons, *Plasmonics* **13** (2018) 2337-2343.

[53] A. Baba, K. Kanda, T. Ohno, Y. Ohdaira, K. Shinbo, K. Kato, and F. Kaneko, Multimode surface plasmon excitations on organic thin film/metallic diffraction grating, *Japanese Journal of Applied Physics* **49** (2010) 01AE02.

[54] G. Perrier, R. de Bettignies, S. Berson, N. Lemaître, and S. Guillerez, Impedance spectrometry of optimized standard and inverted P3HT-PCBM organic solar cells, *Solar Energy Materials and Solar Cells* **101** (2012) 210-216.

[55] C. V. V. M. Gopi, M. Venkata-Haritha, H. Seo, S. Singh, S.-K. Kim, M. Shiratani, and H.-J. Kim, Improving the performance of quantum dot sensitized solar cells through CdNiS quantum dots with reduced recombination and enhanced electron lifetime, *Dalton Transactions* **45** (2016) 8447-8457.

CURRICULUM VITAE

Author's Name Miss Kulrisa Kuntamung

Date/Year of Birth 24 October 1990

Place of Birth Chiang Mai Province, Thailand

Education

2016-2021 Ph.D. (Chemistry), Chiang Mai University, Chiang Mai, Thailand

2016-2021 Ph.D. (Electrical and Electronic Engineering), Niigata University, Niigata, Japan

2013-2016 M.S. (Chemistry), Chiang Mai University, Chiang Mai, Thailand

2009-2013 B.S. (Chemistry), 1st Class Honors, Chiang Mai University, Chiang Mai, Thailand

Scholarships

2009-2018
Full support from Human Resource Development in Science Project (Science Achievement Scholarship of Thailand, SAST)

2017-2018
Financial support from Graduate School of Science and Technology, Niigata University, Niigata, Japan
(Double Degree Program, DDP)

Publication

Kuntamung, K., Yaiwong, P., Lertvachirapaiboon, C., Ishikawa, R., Shinbo, K., Kato, K., Ounnunkad, K., and Baba, A., "The effect of gold quantum dots/grating-coupled surface plasmons in inverted organic solar cells," Royal Society Open Science, 8(3), 2021, 210022.

Oral presentations

Kuntamung, K., Ounnunkad, K., Lertvachirapaiboon, C., Shinbo, K., Kato, K., Kaneko, F., and Baba, A., "Inverted Organic Solar Cells Enhanced by Incorporating Gold Quantum Dots with Metallic Grating Top Electrode," the 27th Annual Meeting of the Material Research Society of Japan (MRS-J 2017), 5-7 December 2017, Yokohama Port Opening Plaza, Yokohama, Japan.

Poster presentations

Kuntamung, K., Ounnunkad, K., Lertvachirapaiboon, C., Shinbo, K., Kato, K., Kaneko, F., and Baba, A., "Improving the efficiency of inverted organic solar cells by incorporating gold quantum dots into the hole-transporting layer," KJF International Conference on Organic Materials for Electronics and Photonics (KJF-ICOMEP 2017), 30 August-2September 2017, Gwangju Institute of Science and Technology, Gwangju, Korea.

Kuntamung, K., Ounnunkad, K., Lertvachirapaiboon, C., Shinbo, K., Kato, K., Kaneko, F., and Baba, A., "Enhanced Performance of Inverted Organic Solar Cells by Incorporating Gold Quantum Dots with Metallic Grating Structure," The 17th International Discussion and Conference on Nano Interface Controlled Electronic Devices (IDC-NICE2017), 11-14 October 2017, Niigata University satellite campus, Niigata, Japan.

Kuntamung, K., Ounnunkad, K., Lertvachirapaiboon, C., Shinbo, K., Kato, K., Kaneko, F., and Baba, A., "Improvement of Inverted Organic Solar Cells by Incorporating Gold Quantum Dots on Metallic Grating Structure," Frontier Solar Cell Seminar, 30 November-1 December 2017, Kanazawa University Satellite Plaza, Kanazawa, Japan.

Kuntamung, K., Ounnunkad, K., Lertvachirapaiboon, C., Shinbo, K., Kato, K., Kaneko, F., and Baba, A., “Improvement of inverted organic thin-film solar cells by incorporation of gold quantum dots/plasmonic systems,” The 65th JSAP Spring Meeting, 2018 (JSAP 2018), 17-20 March 2018, Waseda University, Tokyo, Japan.